Integrated On-chip Magnetic-Based Inductors with Externally Applied DC Magnetic Field for RF and Power Applications

by

Mahmoud Khdour

A Dissertation Presented in Partial Fulfillment
of the Requirements for the Degree
Doctor of Philosophy

Approved November 2014 by the
Graduate Supervisory Committee:

Hongbin Yu, Chair
Michael Goryll
George Pan
Hamdallah Bearat

ARIZONA STATE UNIVERSITY

December 2014

ABSTRACT

Inductors are fundamental components that do not scale well. Their physical limitations to scalability along with their inherent losses make them the main obstacle in achieving monolithic system-on-chip platform (SoCP). For past decades researchers focused on integrating magnetic materials into on-chip inductors in the quest of achieving high inductance density and quality factor (QF). The state of the art on-chip inductor is made of an enclosed magnetic thin-film around the current carrying wire for maximum flux amplification. Though the integration of magnetic materials results in enhanced inductor characteristics, this approach has its own challenges and limitations especially in power applications. The current-induced magnetic field (H_{DC}) drives the magnetic film into its saturation state. At saturation, inductance and QF drop to that of air-core inductors, eliminating the benefits of integrating magnetic materials. Increasing the current carrying capability without substantially sacrificing benefits brought on by the magnetic material is an open challenge in power applications. Researchers continue to address this challenge along with the continuous improvement in inductance and QF for RF and power applications.

In this work on-chip inductors incorporating magnetic Co-4%Zr-4%Ta -8%B thin films were fabricated and their characteristics were examined under the influence of an externally applied DC magnetic field. It is well established that spins in magnetic materials tend to align themselves in the same direction as the applied field. The resistance of the inductor resulting from the ferromagnetic film can be changed by manipulating the orientation of magnetization. A reduction in resistance should lead to decreases in losses and an enhancement in the QF. The effect of externally applied DC

magnetic field along the easy and hard axes was thoroughly investigated. Depending on the strength and orientation of the externally applied field significant improvements in QF response were gained at the expense of a relative reduction in inductance. Characteristics of magnetic-based inductors degrade with current-induced stress. It was found that applying an externally low DC magnetic field across the on-chip inductor prevents the degradation in inductance and QF responses. Examining the effect of DC magnetic field on current carrying capability under low temperature is suggested.

DEDICATION

This work is dedicated to my mother and father, to Tom and Carol Quijada, to Amneris and Salman Salman-Cocco, to my friends and family, and to the friendly people of the Encanto park neighborhood.

ACKNOWLEDGMENTS

This work would not have been possible without the support and trust of my advisor, Prof. Hongbin Yu. I would like to express my deepest gratitude to Prof. Hongbin Yu and to my former advisor the late professor Dieter Schroder. I would also like to thank professor Yong-Hang Zhang for sharing his resources. Also, I would like to thank my group members and colleagues for their support and technical discussions. In particular Hana Liang, Ebraheem Azhar, Arunodoy Saha, and Hao Wu from the electrical engineering department; Reza Vatan from the Physical chemistry department, Makram Abdeqader from the material science department.

TABLE OF CONTENTS

Page

LIST OF TABLES

LIST OF FIGURES

Figure Page

Figure Page

Figure Page

LIST OF SYMBOLS

Symbol	
M_s	Saturation Magnetization
H_k	Anisotropy Field
f_r	Ferromagnetic Resonant Frequency
μ_0	Permeability In Vacuum
H_{eff}	Effective Field
Nd	Demagnetizing Factor
γ	Gyromagnetic Ratio
μ_b	Bohr Magnetron
B^i	Internal Field
B^o	External Field
N	Demagnetization Tensor
R	Resistance
ρ	Resistivity
δ	Skin Depth

Chapter 1

INTRODUCTION

1.1 Background and Motivation

Modern technological trends have continued to call for advances in microelectronic scaling. Additionally, these trends have included integrated functionality with the emergence and growth of the System on Chip (SoC), System in Package (SiP), and Power Supply on Chip (PwrSoC) platforms [1-4]. One of the biggest challenges in realizing such an integrated platform has been miniaturizing passive components. Inductors, being one of the fundamental passive components, do not scale well relative to most electronic elements. Inductance technology has come a long way since the early days of simple metal loops. Throughout the last half century, the industry has seen major engineering strides toward the development of discrete components for printed circuit boards (PCBs). In recent years, inductors have progressed to their most advanced state enabling large scale integration on Si chips [5-8]. These "on-chip" inductors have advanced a variety of applications, but most of their impact has been felt in Radio Frequency (RF) and power applications. Thus, a broader impact of high-performance Si-compatible on-chip inductors means that traditionally established RF and hybrid-RF and power systems (traditionally enabled by large and bulky inductors) would be empowered by these developments. Specific applications may include, but are not limited to DC-DC converters, RFICs for LC filters, multi-core processors, and EMI noise reducers. isolators, circulators, non-reciprocal phase shifters, and tunable components [9, 10].

It is well established that conventional attempts toward scaling inductors on Si are accompanied by a loss in performance. The implementation of on-chip inductors has centered around planar spiral inductors. In terms of miniaturization, air-core on-chip inductors have experienced a substantial decline in performance due to parasitic and inherent losses. Additionally, air-core inductors tend to couple parasitically with conductive Si, thereby leading to magnified disadvantages from high substrate loss, high DC resistance, and poor QF [11]. QF is an important metric for highly integrated inductors because it affects phase noise, channel spacing for wireless applications, and frequency planning for other specialty applications.

Recent trends in the field of on-chip inductors have centered around developing unique strategies for reconciling these scaling vs. performance tradeoffs. One of the predominant strategies has been the integration of magnetic materials onto on-chip inductors. Magnetic materials enhance the permeability around the current-carrying wire. The permeability improvement enhances the inductance and QF. Incorporation of magnetic materials has its challenges and limitations. Applications involving high power density and large DC currents drive magnetic-based inductors toward saturation. At saturation, inductance and QF drop to the level of that of an air-core inductor, offsetting the benefits gained by the introduction of the magnetic material.

One strategy that could represent a major advancement in this field is the integration of an externally applied DC magnetic field to on-chip magnetic-based inductors. Few studies have shed some light on this approach. The use of an external field is potentially groundbreaking, as results of this work have yielded very high quality

factor and peak quality factor resonant frequencies, which are especially exciting for RF and power applications.

1.2 Previous Work

Development of on-chip inductors has progressed within the last few decades with a motivation centered on larger density and higher performance QF. A number of device winding geometries (including but not limited to spiral, stripline, solenoidal, toroidalal, etc.) [12, 13] as well as integration structures (such as stacked or 3D) [14-16] have been reported and thoroughly explored. As previously stated, air-core, spiral inductors are the dominant on-chip inductors in today's technology due to their ease of fabrication and low cost. These features have made them the leading choice in the industry settings. However, spiral air-core inductors tend to exhibit only single-digit nano henry order inductance, contribute to low inductance density. These qualities of air-core inductors make them incompatible with the scaling trajectory of SoC.

Recently, the progression has been towards incorporation of soft ferromagnetic materials into on-chip inductors. The high permeability of these materials can enhance magnetic flux within the inductor, thereby enabling miniaturization to some degree as well as decoupling some substrate losses. Some of the most fundamental works related to incorporation of magnetic material on spiral inductors are enumerated.

A theoretical study by Sullivan et al. established that a single layer magnetic material deposited over an air-core inductor can offer at most twice the increase in inductance [17]. Theoretically, multiple layers can contribute to a large inductance increase, although experimental results have demonstrated challenges achieving these

goals [18-20]. Ni-Fe (permalloy) has been a conventional material of choice in this regard. In 1984, Kawabe et al. demonstrated multiple metal layers sandwiching a permalloy film on SiO_2. However, a low peak QF of 1 and QF frequency (tens of MHz) were resultant due to capacitive losses at the multiple interfaces [21]. Using the same material system in 1992, Yamaguchi et al. created a structure using striplines and saw a 4x increase in inductance with double the QF at an order of magnitude larger frequency than the sandwiched structure [22]. These stripline typologies were then repeated and heavily studied by Koreniviski and Van Dover et al. using both Ni-Fe and Co-Nb-Zr systems in 1997 [11]. Another study on the dimensionality of the stripline configuration was discussed by Yamaguchi et al. (1999) and results demonstrated 7X higher inductance with a peak quality factor at 250 MHz [23, 24]. One important point to note is that these structures have all lacked edge flux closures, which have been described as an important development in mitigation of losses [25].

A number of studies on Co-Zr-Ta films for on chip inductance applications have since been investigated throughout the early to late 2000s. Compared to Ni-Fe based inductors, Co-Zr-Ta films have exhibited fewer resistive losses and a lower permeability, while maintaining a higher saturation magnetization. In 2001, Gardner et al. demonstrated almost 30X increase in inductance using a double-layered spiral inductor with Co-Zr-Ta films [26]. Additionally, the structure incorporated flux-closed techniques which resulted in an inductance densities of 1700 nH/mm^2 with $QF \leq 8$. One of the primary limitations of this design has been the peak quality factor frequency which was in the tens of MHz range. This has made such components unsuitable for RF applications.

Most recently in 2012, Wu et al. demonstrated that the incorporation of Boron led to multiple increases in QF (3.5X) and inductance (3.9X), due the reduction of resistivity that was brought on by the integration of Boron dopants. Furthermore, magnetic vias were also introduced and presented a 30% increase in QF. Additionally, laminations were introduced in this work and a stark improvement in high frequency response was noted over air-core inductors. Laminations act to suppress eddy current losses by adding resistance along their respective directions. The lamination process raised the device inductance by at least 9.1X with 2 GHz range frequency response. Their studies showed that PQ experienced more than a 50% enhancement from 1.5 (non-laminated) to 2.4 (laminated). In the laminated case, PQF had also increased to 500 MHz [27]. In the next year, Wu et al. extended the work by focusing on a 4-turn spiral inductor and explored a variety of lamination techniques that led to a 4.2x increase in inductance and a 5x increase in QF. This work also introduced patterning strategies to modulate film aspect ratio in order to exploit the shape anisotropy effect. They were able to achieve peak QF frequency as high as 1 GHz [28]. In 2014, Wu et al. further detailed the relationship between aspect ratio and saturation field [29] and the role of magnetic vias and their effect on magnetic flux and eddy currents through simulations [30].

1.3 Integration of External DC Magnetic Field

A few studies, have briefly shed some light n introducing external DC magnetif fields to on-chip, magnetic-based inductors [31-33]. This thesis presents a comprehensive study of externally applied DC magnetic fields along the easy and hard

axes of the magnetic film-based the on-chip inductors. This study also considers the role of shape anisotropy while operating the inductor under these conditions. Resistivity (ρ) plays a crucial role in determining the response of QF. A reduction in resistivity leads to a reduction in losses and subsequently an increase in QF response. It is well established that spins in magnetic materials tends to align themselves in the same direction as the external DC magnetic field which leads to changes in electrical resistivity. Changes in electrical resistance in the presence of an externally applied magnetic field were discussed by Zutic et al. [34]. In this work external DC magnetic field was applied to influence the magnetization of the magnetic film. This should result in changes in QF of on-chip inductors as electrical resistivity of the inductor's film should decrease due to the influence of the DC magnetic field. Furthermore, this work was extended to experimentally examine the effect of applying an external DC magnetic field on the inductor's current-carrying capability. This experimental work is expected to lead to an enhancement in current carrying capability.

1.4 Organization of the Document

This section summarizes the work and content of the subsequent chapters. Chapter 2 explores the methods of preparation, fabrication, and characterization of Co-Zr-Ta-B thin film-based inductors. It describes the requirement basis for magnetic-based inductors to integrate with CMOS. Other film characteristics such as demagnetizing factor, lamination, and the role of shape anisotropy through patterning have also been discussed. The fabrication process of the inductors is also described and typologies of inductors including stripline and spiral have been differentiated. Chapter 3 reifies the

merits of applying an external field to the inductor devices. This chapter introduces the testing environments for inductor devices under the presence of external DC magnetic fields. Specific testing equipment used, along with testing configurations have been enumerated. These include field stimulation and the appropriate magnetic field arrangement with respect to the devices' easy and hard axes.

The next several chapters describe the investigation of various responses of stripline inductors to external DC magnetic fields, along the easy and hard axes of the on-chip inductor. Chapter 4 explores the effect of an applied DC magnetic field on inductance for stripline CZTB film inductors. These responses are differentiated for the appropriate stimulation along the easy and hard axes, and they are compared. The physical mechanism that gives rise to their response to the external fields, in the context of the film axial directions is discussed. Chapter 5 investigates the ferromagnetic resonant frequency response of magnetic-based stripline inductors to an externally applied DC magnetic field. The physical mechanism that gives rise to the phenomena is detailed. The responses have been distinguished between applying fields along the easy and hard axis, and an analysis of their response, in terms of their effect on magnetic domains, is discussed. In Chapter 6 the effect of an applied DC magnetic field on Quality Factor (QF) for stripline CZTB film inductors has been explored. Changes in QF by the field applied along the easy and hard axes have been studied and their respective mechanisms have been described. In this analysis, attention is once again given to the differing responses of the devices to field stimulation along both the easy and hard axes. A relationship between the external field and QF is described, via resistance and skin depth. Chapter 7 summarizes the response of inductance, QF, and PQF (desired operating

frequency) to the externally applied DC magnetic fields along both the easy and hard axes. The results and analysis in this chapter are presented as optimization tools for designers to map their desired parameter responses against respective tradeoffs.

In Chapter 8, the response of spiral inductors to externally applied DC magnetic fields is examined. In this study, inductance, QF, and resistance were the factors of analysis. Additionally, the effects of shape anisotropy with spiral inductors have been investigated with and without the DC magnetic field. The relative effects of these considerations on inductance and QF are compared at varying aspect ratios.

Chapter 9 discusses the effects of operating current (DC currents) on spiral inductors. The responses of inductance, resistance, and quality factor, to the current induced magnetic fields (H_{DC}), are enumerated. The degradation effects brought on by H_{DC} is examined, in addition to means for mitigating these effects with an external DC magnetic field. Chapter 10 discusses the effect of an externally applied DC magnetic field in conjunction with a simultaneously applied DC current, on stripline inductors. The inductance and QF response of inductors in this configuration, are explored. The saturation current and the current-carrying limits of the inductor have also been evaluated.

Chapter 11 provides a summary and conclusion of works resulting from this study. A discussion of the broader impact of these results is also presented. Finally, a brief summary and scope of future work is suggested.

Chapter 2

DEVICE FABRICATION

2.1 Introduction

In this chapter a variety of the requirements necessary for magnetic based on-chip inductors will be outlined. The focus of this chapter is to elaborate how these requirements were ultimately realized into devices. These specifications will be the primary framework by which the inductor would be designed and eventually fabricated. Principally, it is important to understand the magnetic characteristics of the films to be incorporated in the system, before they were fabricated into inductor devices. These characterization techniques would otherwise be impossible with small area films on devices. These characteristics are also compared against other films and material systems for optimal device consideration. The details of film deposition and characterization are included, with and without the implementation of other design considerations, such as lamination and patterning. In the next section the device fabrication details are enumerated and differentiation between specific stripline and spiral inductor typologies for this study are discussed in the subsequent section. The testing environment for the devices fabricated via the details in this chapter are discussed in Chapter 3. In it, details regarding the approaches by which these devices were stimulated by an external field and current source are further elaborated.

2.2 Specifications of Magnetic Materials

Any magnetic material used for on-chip inductor fabrication requires a number of minimum criteria. These include high permeability, low losses at the inductor's operating frequency, and ease of integration for CMOS processes. As the overall goal is to drive up performance of scaled inductors for consumer usage, these criteria help to ensure that magnetic materials are indeed beneficial and enable real and measurable performance gains. From a design and systems perspectives, we can further partition these industry needs:

(1) Large saturation magnetization, M_s:

As magnetic films amplify flux, a larger permeability is needed to enhance inductance. At relatively small external fields, the easy axis becomes saturated and utilizes the permeability of the hard axis to describe uniaxial anisotropy. The relationship is described by Kittel et al. [35] as

$$f_r = \frac{\gamma}{2\pi}\sqrt{\frac{M_S H_k}{\mu_0}} \tag{2.1}$$

(2) *Large ferromagnetic resonant frequency (FMR)*:

RF energy tends to absorb at the resonant frequency due the imaginary term of permeability dominating. This effectively transforms the inductor into a resistor. The Kittel equation demonstrates that a higher FMR can be achieved with a larger anisotropy field (H_k), but at the expense of reduced permeability.

(3) *Large resistivity:*

As it has been well established, eddy currents tend to conduct well within ferromagnetic materials, and they represent the most significant loss mechanism at high frequency. Engineering and integrating a high resistivity ferromagnetic material can mitigate these effects, resulting in increased quality factor.

(4) Single domain state:

This ensures the reduction of quality problems associated with the domain of the magnetic material retaining alignment. Changes in the domain pattern often lead to issues with consistent inductance values and magnetic losses.

(5) *Low magnetostriction*:

Having a low magnetostriction can protect against stresses on the film, either from fabrication or normal operation. Stress leads to stress-induced anisotropy, thereby reducing permeability.

(6) Low preparation temperature:

As these magnetic materials often have phase-change properties at low temperatures (around 200 ^{o}C), this can lead to problems with certain processes in the CMOS toolchain that require large temperatures.

2.3 Characterization of Large Magnetic Film - Co-4%Zr-4%Ta -8%B

The magnetic Co-4%Zr-4%Ta -8%B were deposited on a quartz substrate at a thickness of 500 nm via DC magnetron sputtering as described in Wu et al [27]. Boron was included in this composition to increase resistivity (ρ = 115 $\mu\Omega$•cm) compared to CZT films (ρ = 98 $\mu\Omega$•cm). A comparison of magnetic films related to this study (Ni-Fe, Co-Zr-Ta and Co-Zr-Ta-B) is shown below in Table 2.1.

Table 2.1: Comparison of Ni-Fe, Co-Zr-Ta and Co-Zr-Ta-B sputtered films [36]

	Ni-Fe [37]	Co-Zr-Ta [38]	Co-Zr-Ta-B
permeability, μ	650	1000	2
resistivity, ρ ($\mu\Omega$·cm)	20	100	115
FMR (GHz)	0.64	1.4	1.6

In parallel to the deposition, a uniaxial DC magnetic field was applied to the films in order to coordinate magnetic domains, rendering them magnetically anisotropic. These films were then laminated by depositing 100 nm thick CoO through introducing oxygen into the sputtering system. A 500 nm thick non-laminated film was also deposited. A B-H hysteresis loop was obtained measuring coercivity along the easy and hard axis, as seen in Fig. 2.1. It is observed that this coercivity value exceeds that of a single layer film because the magnetization of each layer lies antiparallel with one another, leading to minimum energy considerations. It was also found that the anisotropy field (H_k) increases with smaller lamination thickness and greater number of lamination

layers. A hard axis value of H_k was determined to be 25 Oe and the 10 layer, 50 nm thick laminations resulted in 60 Oe anisotropy field. The laminated films do indeed experience a reduction in permeability at low frequency, because H_k has increased. However, at high frequencies close to FMR, a remarkable increase in frequency response was observed.

(a) (b)

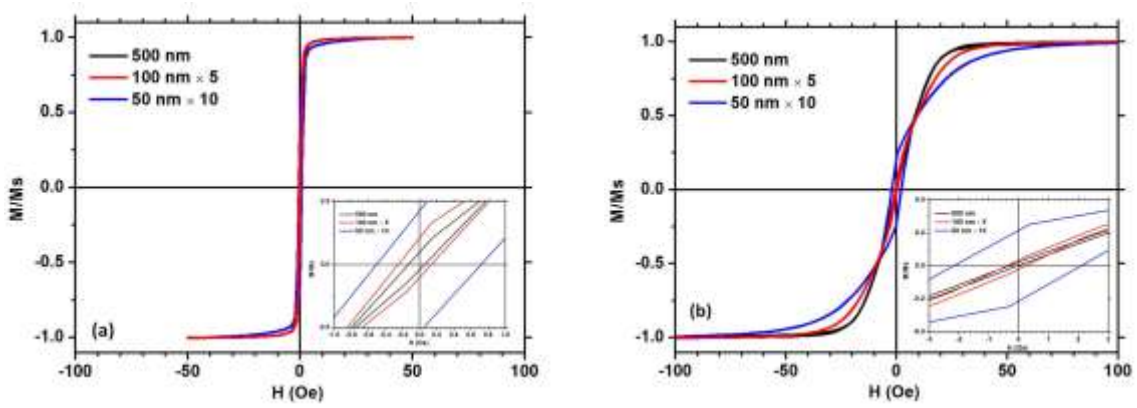

Fig. 2.1: B-H Magnetic Hysteresis Loops For 500 Nm, 100 × 5 Laminated, and 50 × 10 Laminated Thick As-deposited Co-Zr-Ta-B Films Along The (a) Easy Axis And (b) Hard Axis. Insets Show The Coercivity Of Each Film [27]

2.4 Shape Anisotropy Effect on Large Films - Co-4%Zr-4%Ta -8%B

Fabricating patterned and recessed magnetic films has the effect of introducing the shape anisotropy effect by varying aspect ratio. In addition, patterned films are subject to a variety of electromagnetic differences including demagnetizing fields and differing domain structures. The demagnetizing field is one of the most important considerations when dealing with a single domain state magnetic thin film with in-plane anisotropy. In most patterned cases, inductors can expect to see larger QF and larger

operating frequencies due to changes in coercivity (H_c) and permeability (μ) that create variance from flat films. Additionally, the saturation field (H_{sat}) determines the effective permeability of the film but also limits the largest current (saturation current, I_{sat}) that can run through it. Thus, larger saturation fields are directly correlated to larger saturation current [39, 40]. Works that have explored patterned magnetic thin films have demonstrated patterning effects on saturation fields, but have never applied these to inductor applications.

The films were patterned via Electron Beam Lithography (EBL) and a variety of bar structures at different lengths gives rise to varying aspect ratios. As much space allocated between the bars has been allocated toward each film bar, in other words there is a 50/50 areal coverage ratio in these structures. A schematic representation of the device structures and the optical microscopy of the patterned films are shown in Fig. 2.2.

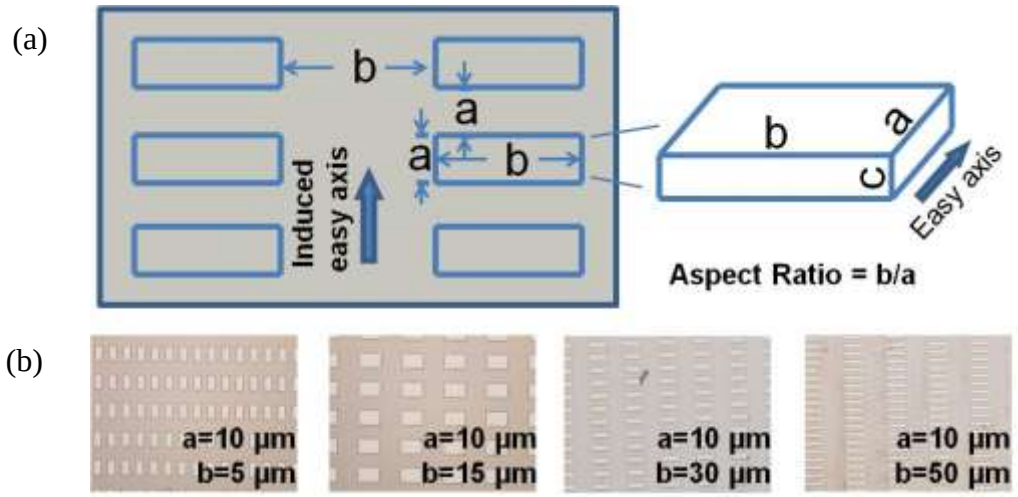

Fig. 2.2: Patterned Co-Zr-Ta-B Films With Varying Aspect Ratios (length/width) With (a) Representation Of Pattern Relative To Device And (b) Optical Microscopy Of Patterned Arrays Varying Aspect Ratios (from Left To Right: 1:2, 1.5:1, 3:1, And 5:1) [36]

By extrapolation of the B-H hysteresis curves, the saturation field of the patterned and un-patterned CZTB films can be evaluated, which is highlighted in Fig. 2.3. In the unaltered case (700 µm x 700 µm), an easy axis saturation field (H_{sat_Easy}) was determined to be 5 Oe and a hard axis saturation field (H_{sat_Hard}) was determined to be 35 Oe. In the patterned case (a regular repeating array of bars), due to shape anisotropy, both saturation fields experience an appreciable increase compared to their unpatterned cases (15 Oe to 500 Oe for H_{sat_Easy}, 40 Oe to 655 Oe for H_{sat_Hard}) [36].

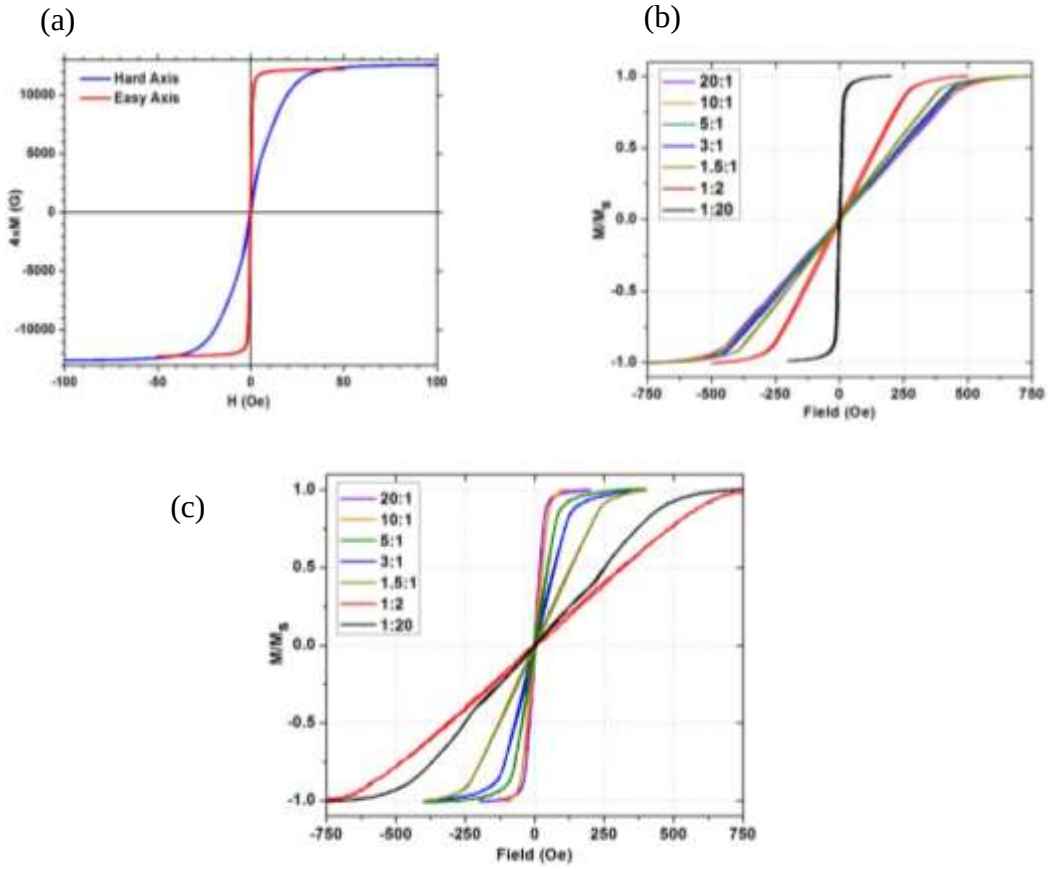

Fig. 2.3: Measured B-H Hysteresis Loop From 100 Nm×5 Laminated Co-Zr-Ta-B Films. (a) 0.7 mm×0.7 mm Un-patterned Film (b) Easy Axis And (c) Hard Axis Of Patterned Films With Varying Aspect Ratios [36]

Additionally, a strong dependence on shape anisotropy depending on the aspect ratio has been observed. For large aspect ratios, the energy from shape anisotropy exceeds that of the induced anisotropy from the uniaxial magnetic field applied in-situ to film deposition. As a result, the expected easy axis has a greater saturation field in comparison to that of the hard axis saturation field. The commonly known easy and hard axes have been reversed around an aspect ratio of 1, and this is clearly delineated in Fig. 2.4.

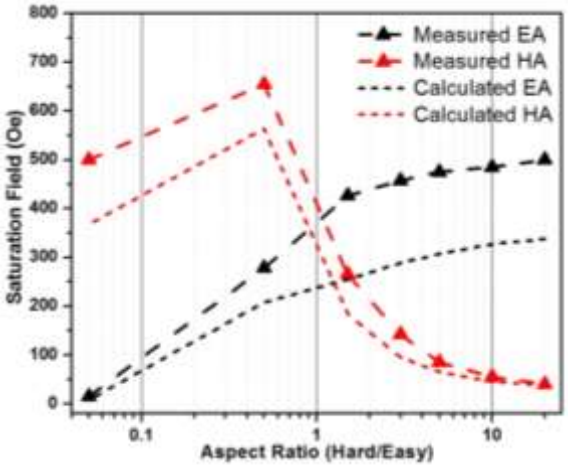

Fig. 2.4: Experimental And Calculated Saturation Filed Of Patterned Magnetic Bars Array In Easy Axis (EA) And Hard Axis (HA) [36]

2.5 Fabrication of On-Chip Magnetic-Based Inductors

The integration of amorphous Co-Zr-Ta-B films on on-chip inductors is summarized. For full integration, refer to [36]. Fabrication commenced with the Cu metallization (200 nm thick through RF magnetron sputtering) of 4-turn spirals (88 μm x 160 μm measured across the outside edge), and a stripline formation (450 μm long, 46 μm wide) on quartz substrates. Electron beam lithography (EBL) was used to pattern the 5 μm wide Cu lines and spirals, and a baseline inductance for spiral structures was established to be 1.9 nH. An insulating layer of polyimide was then deposited in order to electrically isolate the copper lines from the subsequent magnetic films. As described in section 2.2, 500 nm of amorphous Co-4%Zr-4%Ta-8%B alloy films (determined by GHz range skin depth[41]) were sputtered on top of the patterned formations and were joined by magnetic vias. The vias served to maximally enhance flux and form a continuous magnetic circuit. For stripline inductors, non-laminated, as well as laminated films were

deposited on top of the inductor structures for comparison. In the laminated case, 5 layers of 100 nm thick Co-O film laminations were incorporated to reduce eddy currents and the skin effect, as described in section 2.1. For spiral inductors, laminated films were deposited atop inductor structures for subsequent analysis.

2.6 Losses and Patterned Magnetic Vias

Magnetic vias were introduced to mitigate the effect of eddy currents on inductor performance. The relative effects of vias were comprehensively explored by Wu et al., in which they investigated inductor performance by modulating the width, shape, and patterning of the magnetic vias [36]. Through optimization efforts from experimental and simulated (using HFSS 3D software package) work, the final design of these vias, demonstrated that unpatterned films with fingered vias resulted in the best performance [29]. This is due to the design of finger-shaped geometries eliminating eddy current loops along their respective distribution, while maintaining a continuous magnetic flux. A schematic of inductor devices with and without finger-shaped vias on a spiral inductor are shown below in Fig. 2.5.

Fig. 2.5: Schematic Of Spiral Inductors (a) Without And (b) With Finger-shaped Magnetic Vias.

Inductors incorporating finger-shaped vias had larger PQ and larger PQF. The combined results of fingered vias and laminating have demonstrated the capacity for these inductor structures to have high performing QF response. These performance characteristics were precisely why this class of devices were chosen for the study of externally applied DC magnetic fields on on-chip magnetic-based inductors.

Chapter 3

EXTERNALLY APPLIED DC MAGNETIC FIELD STUDY

3.1 Introduction

In the previous chapter, on-chip inductors incorporating magnetic films were introduced. The major enhancements to inductance and quality factor were highlighted. It is important to note that these measurements were collected without the presence of an external magnetic field. Utilizing magnetic films in inductors increases the inductance density, which is the key requirement to realize the ultimate monolithic system on-chip reality. These may include the realization of on-chip and on-die transformers. For the on-chip magnetic-based inductors to be the gateway for the complete system on-chip, they need to have high current-carrying capabilities, a milestone that is currently challenging researchers in the field and has yet to be overcome. On-chip magnetic-based inductors have very poor current carrying capability. Inductor's magnetic film saturates at low current value, I_{sat}. At saturation, the inductor loses the advantages of having magnetic film as the inductance value becomes that of air-core inductor. Therefore, the challenge of developing a good quality and highly dense inductor with large saturation current requires continued effort.

The response of magnetic domains in a magnetic films to an externally applied magnetic field, otherwise referred to as the susceptibility, is a measure of how responsive magnetic domains are to an externally applied magnetic field. Hence, the idea of integrating a DC magnetic field with magnetic-based inductor should influence the

susceptibility, and subsequently the permeability and the current carrying capability (or the saturation current) as it will be discussed in the future chapters. Therefore, studying the effect of externally applied magnetic fields on magnetic-based on-chip inductor, in addition to understanding their effect on current carrying capability is of our interest.

3.2 Experimental Setup

Magnetic thin-film inductors were characterized with HP 8720D network analyzer with cascaded GSG probes. The DC magnetic field was introduced by the placement of two permanent magnets across the device, and the field was measured using a magnetic probe. The DC magnetic field was applied along the easy axis (EA) and the hard axis (HA) independently. For the EA case, the permanent magnets were placed across the device to exert a DC magnetic field parallel to the easy axis of the inductor's thin film, as seen in Fig. 3.2, we refer to this case as H(Easy). On the other hand, in the HA case, the permanent magnets were placed across the device to exert a DC magnetic field perpendicular to the easy axis of the inductor's thin film, as seen in Fig. 3.3, we refer to this case as H(Hard). To obtain different DC magnetic field values, a reference point for the magnets was first ascribed on the testing arrangement, and the magnets were subsequently displaced at predetermined positions to modulate field strength.

For these devices, the current runs parallel to the easy axis. Therefore, the AC current, or the RF signal, supplied by the HP 8720D network analyzer, induces a small magnetic field that is always parallel to the hard axis.

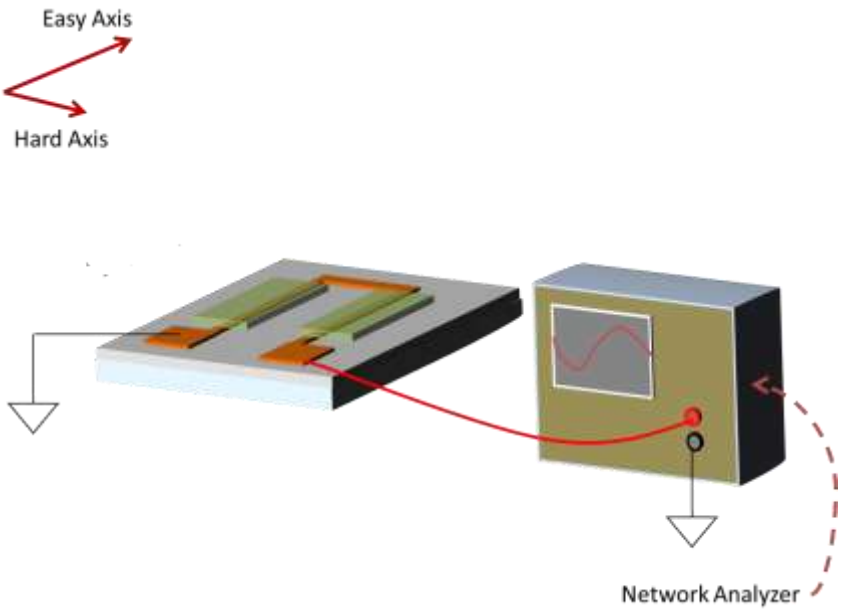

Fig. 3.1: Test Setup Without External Source

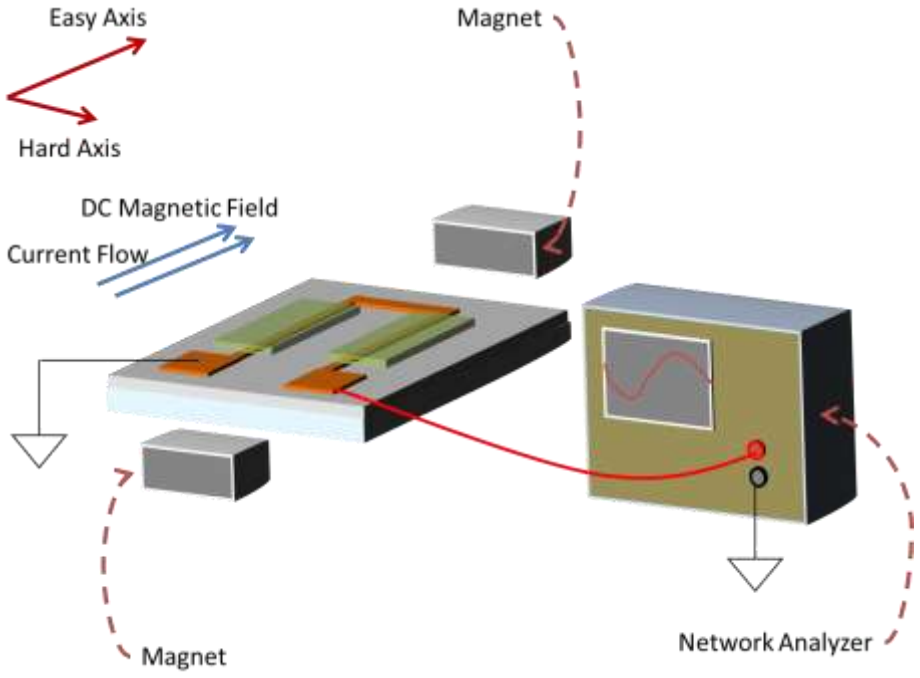

Fig. 3.2: Test Setup for H(Easy) Case

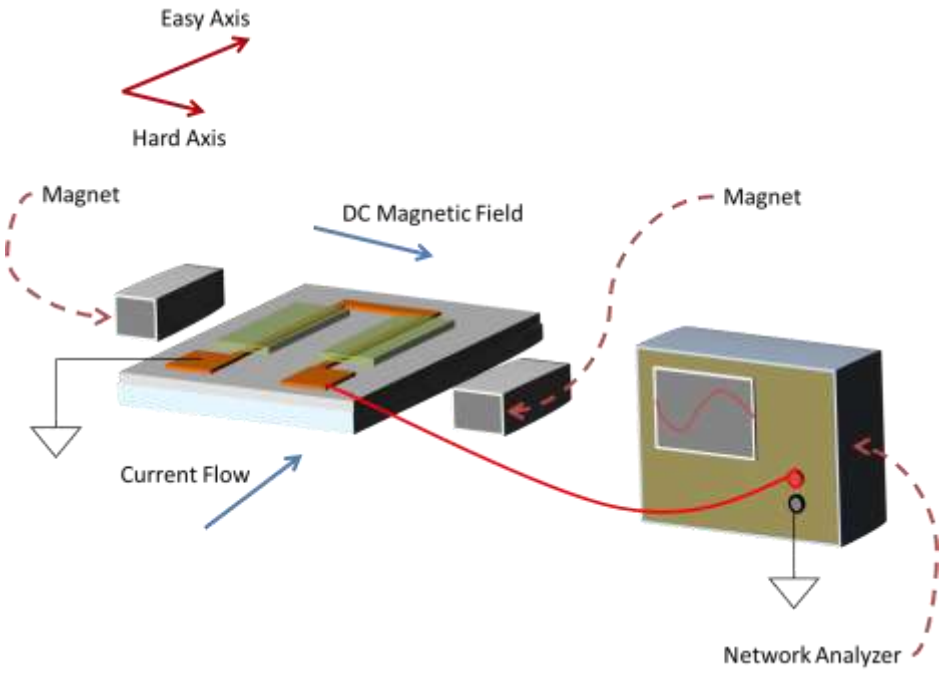

Fig. 3.3: Test setup for the H(Hard) Case

To examine the inductor's current carrying capability and to study the effect of different currents on the characteristic of magnetic-based inductor the AC signal provided by the HP 8720D network analyzer was superimposed on a DC current via a Bias-Tee shown in Fig. 3.4. The DC current was supplied by Keithley source meter. The current flow is parallel to the easy axis, and the plane of current-induced magnetic field, H_{DC}, is parallel to the hard axis.

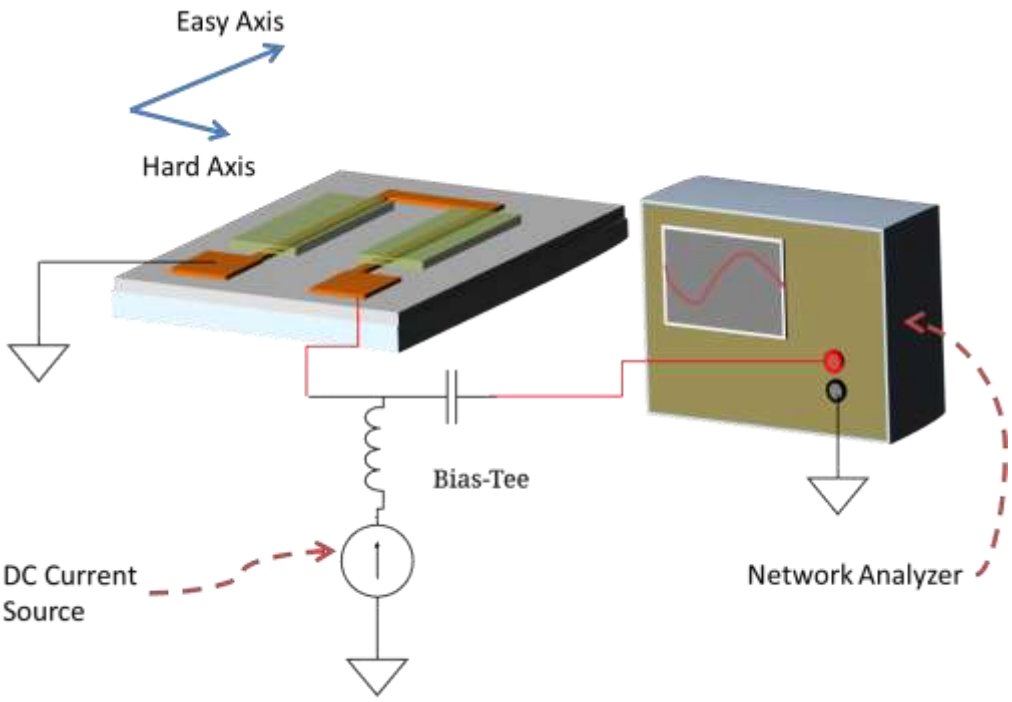

Fig. 3.4: Test Setup to Examine Current Carrying Capability

To examine the influence of the externally applied DC magnetic field on the device current carrying capability, or the saturation current (I_{sat}), both DC magnetic field and DC current were applied simultaneously, as in Fig. 3.5. For a given DC magnetic field value the DC current was varied by 5 to 10 mA every 10 seconds. It is to be noted that the DC current was reset to zero before each trial. The DC magnetic field was then varied by reducing the distance between the magnets by moving each a predetermined length. The DC magnetic field was then measured by magnetic Hall probe and the DC current was varied for the new field, as was done for the prior field.

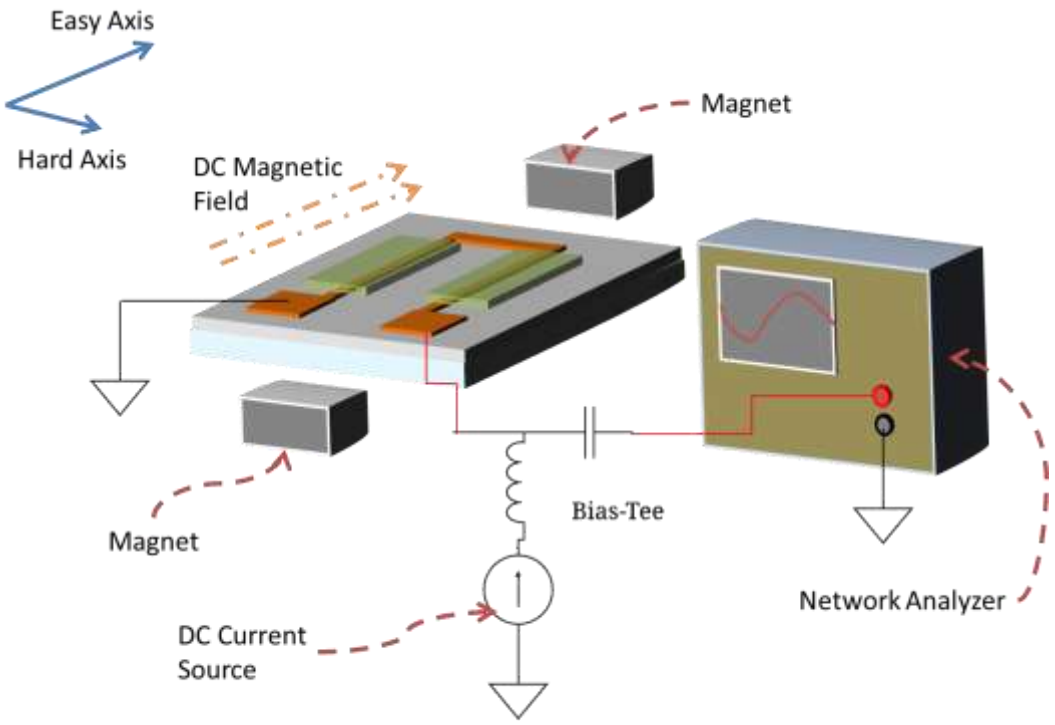

Fig. 3.5: Test Setup To Examine The Effect Of Dc Magnetic Field On The Device's Current Carrying Capability

In the testing configuration, the easy axis is defined along the vertical axis, and hence, the externally applied field H_{DC} is defined parallel to it. Consequently, the hard axis is oriented along the lateral axis and the AC current-induced field, H_{AC}, runs parallel to it.

Chapter 4

INDUCTANCE RESPONSE TO DC MAGNETIC FIELD

4.1 Introduction

Externally applied DC magnetic fields effectively align the magnetic domains and exert a force on them that leads to a decrease in their susceptibility to the AC current-induced magnetic field, H_{AC}. Furthermore, this decrease in susceptibility leads to a reduction in permeability and subsequently a reduction in inductance. The reduction in susceptibility continues with further increases in the externally applied field until the DC magnetic field overpowers the magnetic domains to the point that their response to H_{AC} becomes negligible. Under such conditions, the susceptibility drops to negligible values and the permeability drops to the air-core value. Subsequently the inductance value becomes that of air-core inductor; this is what we refer to as the saturation state. Operating in the saturation state defeats the purpose of integrating magnetic materials to air-core inductor. This section will thoroughly detail the effect of applying an external DC magnetic field along the easy and hard axes of a stripline on-chip inductor. For both, the easy axis case, H(Easy), and the hard axis case, H(Hard), inductance decreases with increases in the field value. But inductance does not change for low to moderate field values in the H(Hard) case due to the shape anisotropy effect. The inductance then reaches somewhat of a steady state value for the H(Easy) state at large fields due to the presence of edge domain effect.

4.2 Inductance Response to DC Magnetic Fields along the Hard Axis

Externally applied magnetic fields along the hard axis, H(Hard), of stripline inductors, Fig. 4.1, influences the response inductance as it is reflected by the data in Fig. 4.2. For low to moderate field value (12 Oe to 125 Oe), inductance response along the entire frequency range does not change. For large area CZTB film, the saturation field along hard axis is around 20 Oe, as shown in Fig. 4.2 (a), thus even after applying 125 Oe the film in the inductor has not started to saturate. This is due to the fact that stripline inductors have the geometry of a long length (L = 432 um), compared to their short width (W = 11 μm). This geometry leads to an inductor with a large aspect ratio, (L/W), which subsequently results in an pronounced shape anisotropy effect along the easy axis. For low to moderate field values the magnetic domains are governed by the shape anisotropy effect, therefore the response of magnetic domains to the AC current-induced magnetic field, H_{AC}, does not change. Hence, there are no changes in susceptibility and permeability, and subsequently no changes in inductance for low to moderate fields (0 Oe to 125 Oe), as it is reflected in Fig. 4.2.

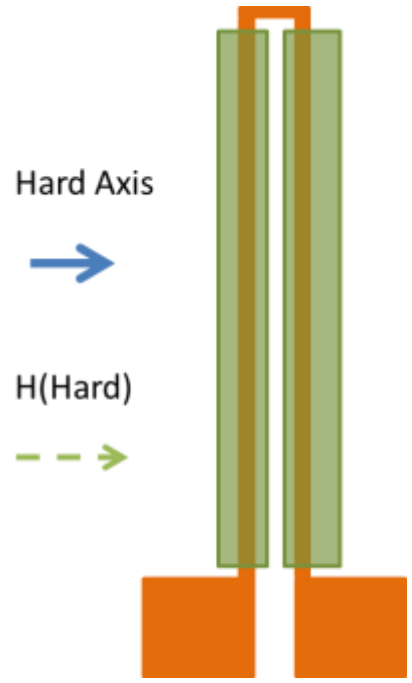

Fig. 4.1: H(Hard) Applied on Stripline Inductor

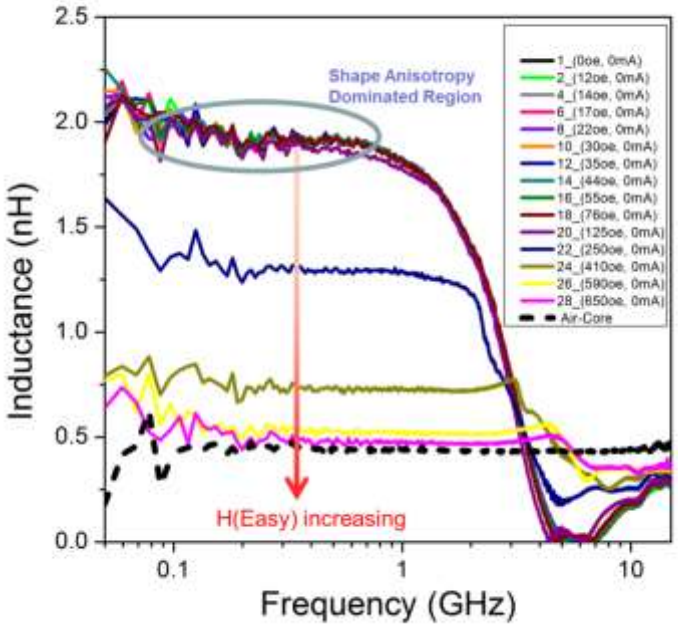

Fig. 4.2: Inductance Of Single-turn Stripline Inductor With Complete Co-Zr-T-B Film Under Different H(Hard) Field Biases.

At some point, however, the increasing applied field overcomes the shape anisotropy effect and becomes the dominating factor. The field value at this point is defined as the threshold field, H_{Th}. For stripline inductors, H_{Th} is at 125 Oe, and Fig. 4.2 shows that inductance decreases with increasing field values above the threshold field, H_{Th}. Operating the inductor above H_{TH} shifts the magnetization toward the hard axis to become within an angle of the plane of the AC current-induced magnetic field, H_{AC}. This shift, along with the exerted force on the magnetic domains by the increased magnetic fields reduces the response of magnetization to H_{AC}. Therefore, the susceptibility decreases and subsequently the permeability and inductance.

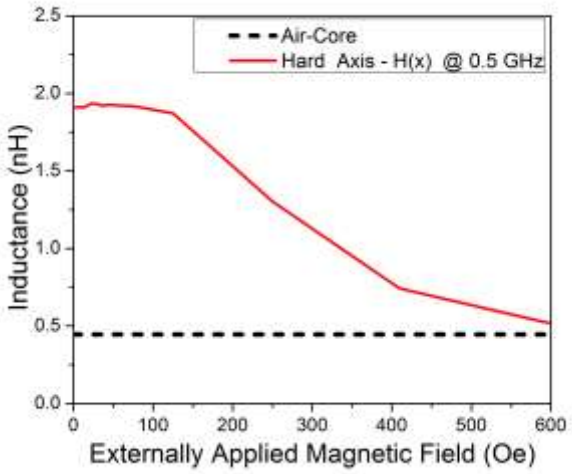

Fig. 4.3: Inductance At Operating Frequency Of 0.5 GHz Of Single-turn Stripline Inductor With Complete Co-Zr-Ta-B Film Under Different H(Hard) Field Biases.

At very large fields magnetic domains become perpendicular to the easy axis and become parallel to the plane of the AC current-induced magnetic field, H_{AC}. The majority of magnetization within the film covering the Cu wire (11 μm in width) becomes parallel to H_{AC}. Magnetic domains in the remaining portion of the surface film (2 x 8 μm, 16 μm in total width), and within the magnetic via are within angles to the plane of H_{AC} field,

due to the natural shape of the current-induce magnetic field, H_{AC}. Whether parallel to H_{AC} or not, magnetic domains are within the same plane as H_{AC}. At some point, the orientation of magnetic domains along with the force exerted on the magnetic domains (by a very strong magnetic field) results in magnetic domains becoming non-responsive to H_{AC}. Therefore, the susceptibility becomes zero and subsequently the permeability drops to the free space value, μ_o, resulting in an inductance drop to air-core values. This is the definition of the saturation state. The stripline inductor reaches its saturation state at an applied field of 650 Oe, as it is reflected in Fig. 4.2 and Fig. 4.3.

4.3 Inductance Response to DC Magnetic Fields along the Easy Axis

Externally applied magnetic fields along the easy axis, H(Easy), of the stripline inductor, Fig. 4.4, influence the inductance response, as indicated in Fig. 4.5. Unlike the H(Hard) case, the anisotropy field due to shape of the magnetic film on inductor is in the same direction as the applied external field, thus it runs parallel to it as shown in Fig. 4.4. Before applying an external magnetic field to the inductor, magnetic domains are in semi-equilibrium, as shape anisotropy results in partial magnetization along the easy axis. In this case, some magnetic domains are positioned along the easy axis, and others can easily align toward the easy axis by simply applying a small external field, H(Easy). Therefore, small fields exert forces on magnetic domains and reduce their response to the H_{AC} resulting in small reduction in susceptibility and subsequently small reduction in permeability and inductance.

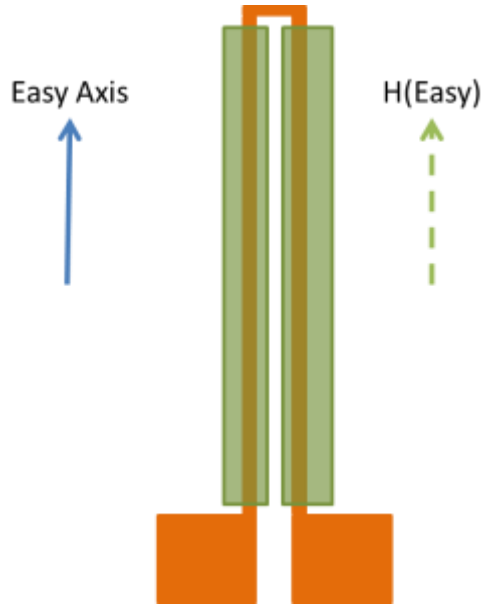

Fig. 4.4: H(Easy) Applied on Stripline Inductor

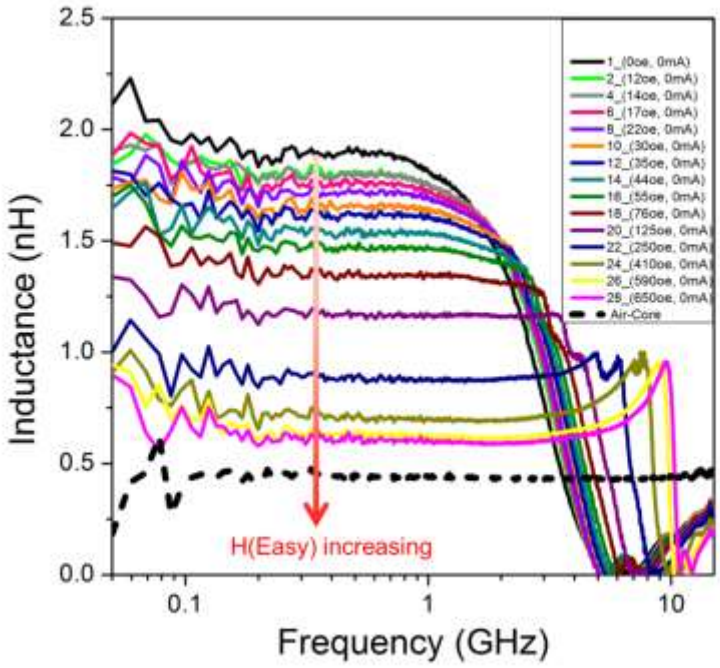

Fig. 4.5: Inductance Of Single-turn Stripline Inductor With Complete Co-Zr-Ta-B Film Under Different H(Easy) Field Biases.

Further increases in the applied field exert stronger forces on the magnetic domains, hence hindering their response to the AC current-induced magnetic field, H_{AC}. This leads to further decreases in susceptibility and subsequently further decreases in permeability and inductance, Fig. 4.5 and Fig. 4.6. At very large fields, near saturation, majority of magnetic domains (except the edge domains) are in parallel to the easy axis and are under the influence of a strong force exerted by the large fields. The edge effect plays a significant role in the H(Easy) case due to the easy axis running along the long length (L_{mag}) of the stripline inductor (L_{mag} = 480 μm). Therefore, for the large fields near the saturation (650 Oe), the edge effect overcomes the applied field and its influence on the susceptibility of magnetic domains to H_{AC} diminishes, resulting in a reduction in inductance with the applied field. Unlike the H(Hard) case, at 650 Oe inductance does not reach saturation, rather it is reduced to a value that was still 50% above the saturation value (or air-core). Further studies are required to explore the edge effect and saturation at much larger fields.

At very large H(Easy), the magnetic domains (except edge domains) become completely dominated by H(Easy), that is they become unresponsive to H_{AC}. Hence, the susceptibility drops to values reflecting the susceptibility of edge domains to H_{AC}. This is the point at which the film becomes fully saturated along the easy axis and the inductance value becomes very close to that of an air-inductor.

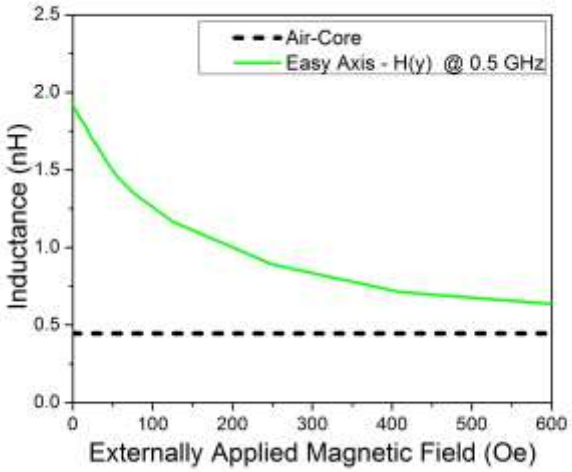

Fig. 4.6: Inductance At Operating Frequency Of 0.5 Ghz Of Single-turn Stripline Inductor With Complete Co-Zr-Ta-B Film Under Different H(Easy) Field Biases.

4.4 Inductance Response to DC Magnetic Fields along Hard vs. Easy Axes

The response of inductance to an externally applied field along the easy and hard axes is illustrated in Fig. 4.7. For low to moderate fields, H(Hard) is dominated by the shape anisotropy effect, and for very large field values H(Easy) is dominated by the edge effect. Beyond these regions, H(Easy) and H(Hard) experience a decrease in inductance with increases in the externally applied magnetic fields.

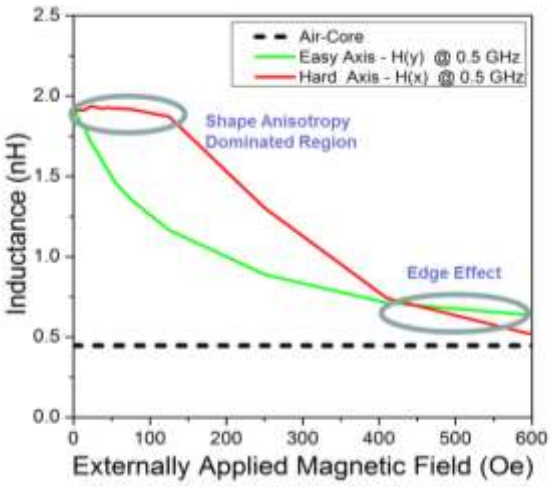

Fig. 4.7: Inductance Of H(Easy) Vs. H(Hard) At Operating Frequency Of 0.5 Ghz Of Single-turn Stripline Inductor With Complete Co-Zr-Ta-B Film.

For the stripline inductor, the inductance response to an externally applied magnetic field along the hard axis (H(Hard)) is summarized in Fig. 4.3 for an operating frequency of 0.5 GHz. For low to moderate H(Hard) values (0 Oe to 150 Oe), inductance response is dominated by the shape anisotropy effect. When H(Hard) exceeds 125 Oe, inductance decreases as H(Hard) continues to increase. This persists until the magnetic film completely saturates at 650 Oe. Hence, the inductance value becomes that of air-core inductor, 0.48 nH.

The inductance response to an externally applied magnetic field along the easy axis (H(Easy)), for an operating frequency of 0.5 GHz, is summarized in Fig. 4.4. Inductance starts to decrease with introduction of low field values as there is no shape anisotropy effect to overcome. Rather, unlike the H(Hard) case, saturation is not attained at 650 Oe. At 650 Oe, the inductance value is 50% above that of the air-core value as noted in Fig. 4.5 and Fig. 4.6. Furthermore, at large field of H(Easy) the rate at which inductance decreases is reduced significantly.

Chapter 5

FERROMAGNETIC RESONANT FREQUENCY RESPONSE TO DC MAGNETIC FIELD

5.1 Introduction

Ferromagnetic resonant frequency (FMR) is related to the rotational motion (precession) of magnetic moments. Externally applied magnetic fields exert torque on magnetic moments, causing them to precess. FMR, arises from the precessional motion of the magnetization, M. The precessional frequency depends on the strength of the magnetic field. Therefore, as the externally applied magnetic field increases, FMR increases for both cases: the applied magnetic field along the hard axis, H(Hard), as noted in Fig. 4.7, and the applied magnetic field along the easy axis, H(Easy), as demarcated in Fig. 4.4 The magnetization precession in magnets under magnetic fields is described by the Bloch equation (equation 5.1), and is illustrated in the representation of the phenomena in Fig. 5.1:

$$\frac{dM}{dt} = \gamma M x B^i = \gamma M x (B^0 - NM) \quad (5.1)$$

where $\gamma = \frac{g\mu_B}{h} = 9.274x10^{-23} JT^{-1}$ denotes the gyromagnetic ratio

μ_B is the Bohr magnetron

B^i is the internal field

B^o is the external field

N is the demagnetization tensor

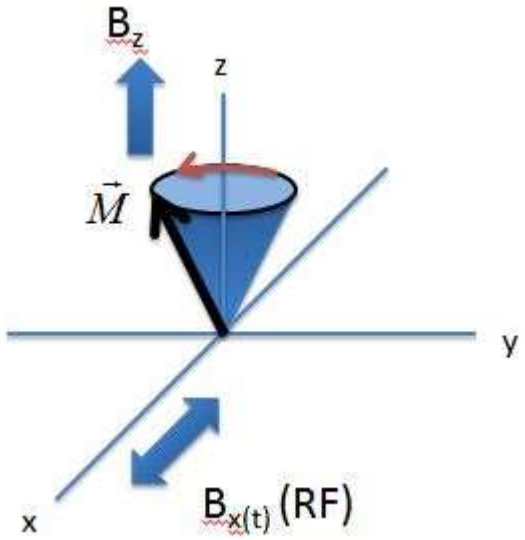

Fig. 5.1: Magnetization Precession In Magnets Under Magnetic Fields, Bz External DC Magnetic Field, Bx(t) Is The Ac Current Induced Magnetic Field, H_{AC}

Utilizing equation 5.1 while accounting for the shape anisotropy effect, the FMR frequency is governed by equation 5.2

$$\omega_0^2 = \gamma^2\left[B_0 + \mu_0 H_k + \left(N_y - N_z\right)M_0\right] \quad (5.2)$$

Where B_0 the external field,

H_k the shape anisotropy effect,

and N is the demagnetization tensor.

FMR increases with the increase in externally applied DC field, and also with the increase in the shape anisotropy effect. In the case of an applied DC magnetic field *parallel* to the magnetic film, MRF response is governed by equation 5.3

$$N_x = N_z = 0, N_y = 4\pi \rightarrow \omega_0 = \gamma\sqrt{B_0 + \mu_0 H_k + 4\pi M_0} \quad (5.3)$$

5.2 FMR Response to DC Magnetic Fields along the Easy Axis

For the case of applying DC magnetic field along the easy axis, H(Easy), the shape anisotropy effect does not oppose the applied field, rather it runs parallel to it, which is in the same direction as the easy axis. Hence there is no shape anisotropy dominated region, as there was in the H(Hard) case. Magnetic domains are thus easily responsive to low fields. Subsequently, changes in FMR response is reflected for low fields (i.e. 12 Oe) and beyond, shown in Fig. 4.5 and Fig. 5.3. As H(Easy) increases, the precession frequency increases, and subsequently the FMR increases via equation 5.3.

The inductance response across the entire frequency range for various applied fields is shown in Fig. 4.5. FMR was defined to be the frequency at which the rolloff in inductance takes place and it was extracted from Fig. 4.5. This extraction is represented in Fig. 4.2 with FMR represented by the black trace. Likewise, the resistance response for the same measurement is shown in Fig. 4.12. As the system approaches the resonance state the resistance increase and reaches a maximum value, peak resistance (PRs), at a peak resistance frequency (PRsF), represented in Fig. 4.12. PRsF is the exact FMR value at which inductance is at its lowest state and resistance at its apex.

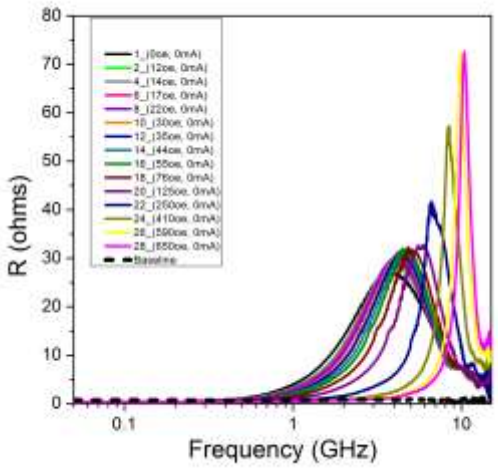

Fig. 5.2: Resistance Response To Varying Fields Along H(Easy)

The difference between the PRsF (red trace) and FMR (black trace) seen in Fig. 5.3, and is simply a product of the definition to FMR during its extraction from Fig. 4.5. If we are to define FMR to be the point for which inductance at its lowest value rather than being the rolloff point in inductance value, FMR will have the same value as PRsF. What is worth noting here is that FMR increases with increases in the externally applied DC magnetic field, (from 2 GHz to 10 GHz) for an for an H(Easy) values up to 650 Oe, which agrees with the FMR response as noted in equation 5.3. Future research is required to study the response of FMR with very strong fields along the easy axis.

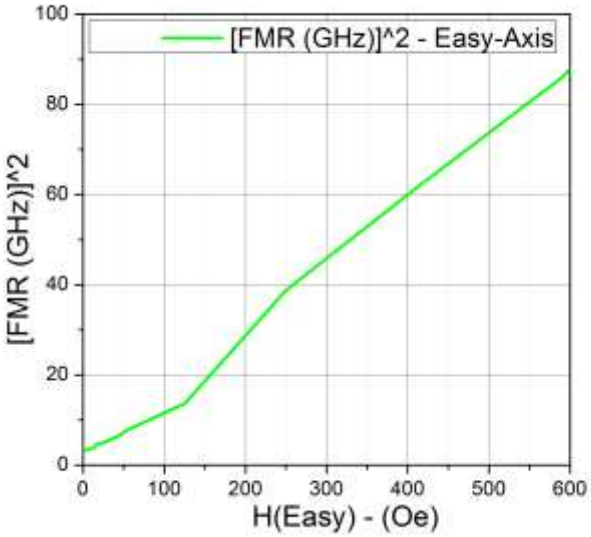

Fig. 5.3: Peak Resistance Frequency (PSRF) And FMR Vs. Field Strength Along The Easy Axis

5.3 FMR Response to DC Magnetic Fields along the Hard Axis

To examine the response to FMR along the hard axis, an externally applied magnetic field was applied along the hard axis of the stripline inductor as shown in Fig. 5.31. The frequency response of FMR at very low and high fields has been examined and analyzed.

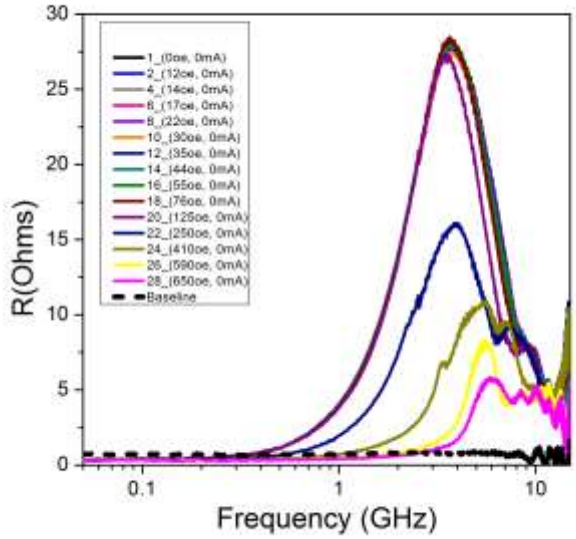

Fig. 5.4: Resistance Response To Varying Fields Along H(Hard)

The definition and extraction of FMR and PRsF is detailed in section 5.1. FMR and PRsF increase with increases in applied field. In this case, FMR does not change for low to moderate fields as noted in Fig. 5.52. This region of field-independent domain is due to shape anisotropy domination. At some point, the externally applied magnetic field along the hard axis overcomes the shape anisotropy effect and becomes the dominant force. H_{TH}, in this case, is measured to be 125 Oe for the stripline inductor. As the applied field increases beyond the threshold value, FMR increases with the increase according to the same physics that governed section 5.1. These results are illustrated in the transition of a field-independent FMR of 1.2 GHz to a field-dependent FMR with values of 2.0 GHz for 250 Oe, 3 GHz for 410 Oe, and 4.8 GHz for 650 Oe (Fig. 5.5).

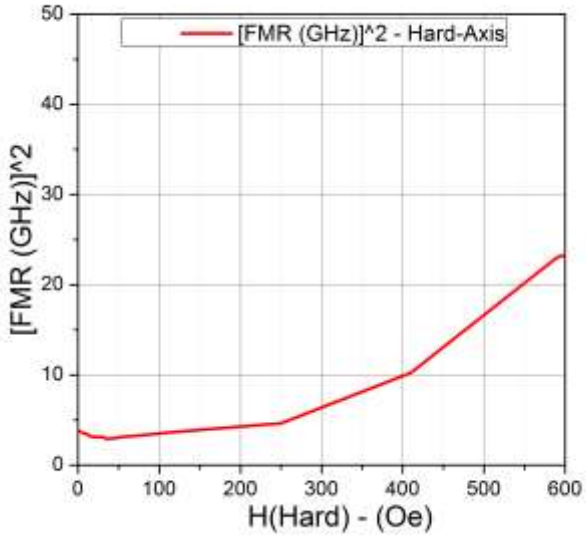

Fig. 5.5: Peak Resistance Frequency (PSRF) And FMR Vs. Field Strength Along The Hard Axis

For applied fields near the saturation point (590 Oe, 650 Oe), magnetic domains become parallel to the DC applied magnetic field, and to the plane of AC current-induced magnetic field (H_{AC}). Hence, the effective field (H_{eff}) is at its maximum value, and the magnetization (M) is parallel to H_{eff}. Just as equation 5.1 describes, when M is parallel to $H_{eff,}$ the curl product reflects that the precessed motion of M will cease to exist. Furthermore, there are no edge domains to play a role in FMR as the case for H(Easy). The combination of these two points could be the reason behind the reduction in the peak resistance, PRs, for the H(Hard) case, Fig. 5.4. Future research is required to study the response of FMR, along the hard axis, under very strong field values (at saturation and beyond). That experiment should deliver insight into the behavior of magnetic-based inductors.

5.4 FMR Response to DC Magnetic Fields along Hard vs. Easy Axes

The difference in FRM and PRsF responses for the H(Easy) and H(Hard) cases are summarized in Fig. 5.6. FMR for the H(Easy) case is presented in the black trace, and FMR for the H(Hard) case is presented in the green trace. Increase of FMR with subsequent increases in the applied DC magnetic field is governed by the physics in section 5.1. For the H(Hard) case, FMR remains relatively constant for low to moderate fields due to the domination of shape anisotropy. An increase in FMR subsequently leads to an increase in operating frequency, as it has been discussed in Chapter 6, hence applying the DC magnetic field along the easy axis results in a larger increases in the operating frequency.

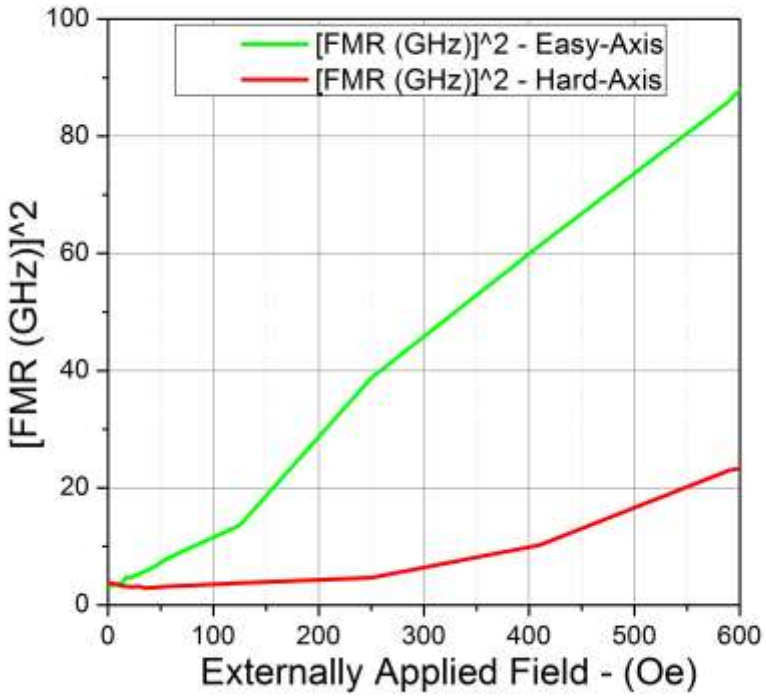

Fig. 5.6: FMR For Various Applied Fields In Both the H(Easy) and H(Hard) Cases

Chapter 6

QUALITY FACTOR RESPONSE TO DC MAGNETIC FIELD

6.1 Introduction

It is well established that spin in magnetic materials tend to align themselves along the same direction as the externally applied magnetic field, which leads to changes in electrical resistivity. Julliere's study of the tunneling between ferromagnetic films shows that resistance can be changed by manipulating the orientation of magnetization [42]. Changes in electrical resistance in the presence of an externally applied magnetic field were discussed by Zutic et. al. [34].

In this study spin is viewed as the average spin of an ensemble of electrons expressed by magnetization (M). An external DC magnetic field was applied to influence the magnetization of the inductor's magnetic film. This should lead to changes in quality factor, as changes in the electrical resistance of magnetic films are brought on by the externally applied DC magnetic fields.

In Chapter 5 it was discovered how FMR increases with the increase in the applied magnetic field. Increases in FMR lead to the increase in operating frequency, QF, and PQF as will be discussed in this chapter. At low frequencies the response of QF from the relationship in equation 5.1, is not dominated by skin depth or resistance (losses). Rather it increases with the increases in frequency. For reference, the skin depth parameter is defined as

$$\delta = \sqrt{\frac{\rho}{\pi * \mu * f}} \quad (6.1)$$

Where ρ is resistivity, and f is the applied frequency. As frequency increases, a reduction in skin depth is observed according to equation 6.1. The low frequency region is denoted as LFR. The LFR of the QF response in Fig. 6.1 is the range of frequencies below the PQF value. For the measurement without an externally applied magnetic field, the LFR region is 0.3 GHz and below. This reduced skin depth causes the resistance to increase, according to equation 6.2

$$R = \frac{\rho\, l}{W\delta*(1-e^{-t/\delta})} \quad (6.2)$$

The increases in resistance R, ultimately causes a drop in QF, as it is defined below

$$QF = \frac{2\pi f l}{R} \quad (6.3)$$

The LFR region ends when QF reaches its maximum value of PQ. That is when the skin depth and resistance (losses) dominate the QF response as the skin depth decreases with increases in frequency as applied to equation 6.1, lead to increases in resistance noted in equation 6.2, and subsequently a reduction in QF from equation 6.3. Therefore, increasing the range of the LFR region should lead to larger PQF and QF responses, which is a highly desirable enhancement. Applying an external DC magnetic field results in an expansion of the LFR region, which will be discussed later in this chapter.

6.2 Quality Factor Response to DC Magnetic Fields along the Hard Axis

As discussed in section 4.3 the case of applied field along H(Easy) has no shape anisotropy dominated region. Hence, PQ and PQF response for low fields (i.e. 12 Oe), increases as the applied DC magnetic field increases (illustrated in Fig. 6.1). Though, just as in the case of applied H(Hard) field, for low frequencies (0.3 GHz and below) the quality factor decreases with larger applied field. This is not expected, as increases in applied field lead to a decreases in the permeability, thereby leading to increases in skin depth from equation 6.1. This subsequently reduces eddy current losses and increases the QF. This contradiction between the QF response at low frequencies and equation 6.1 remains an open question.

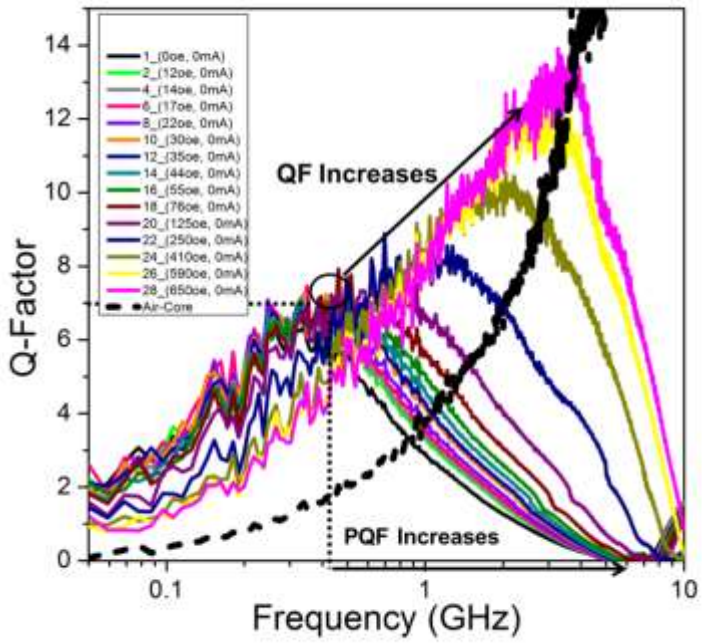

Fig. 6.1: QF For Stripline Inductors With A Field Applied To The Easy Axis

An increase in FMR significantly expands the range of operating frequencies. More significantly, the externally applied DC magnetic field reduces the resistance response at high frequencies. The larger the applied field is, the higher the frequency for which resistance value is suppressed due to the presence of the magnetic field, as noted in Fig. 6.2.

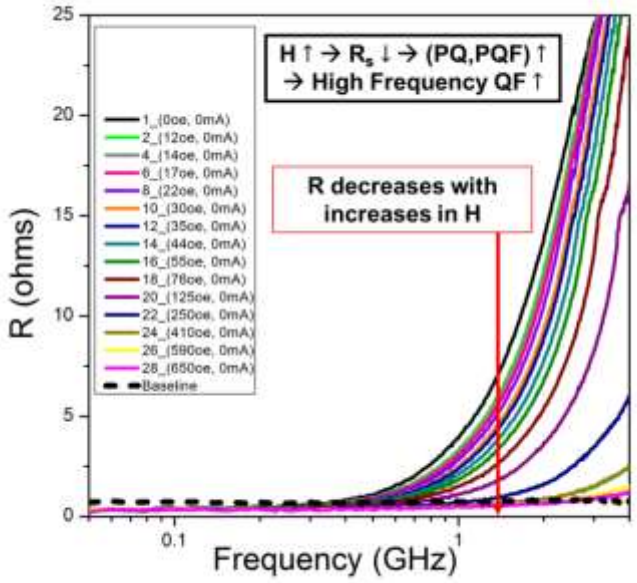

Fig. 6.2: Resistance Response To Varying Fields Along H(Easy)

The reduction of resistance due to a given applied field results in a new PQ and PQF value. A relationship between QF response, Fig. 6.1, and resistance response, Fig. 6.2, governs the PQ, PQF, and resistance. At low frequencies the resistance under a given field is equal to that of air-core resistance. PQF is not only the frequency at which QF is at its peak value (in Fig. 6.1), but it is also the frequency at which the resistance of the magnetic-based inductor overcomes the resistance of the air-core inductor, (seen in Fig. 6.2). Increasing the externally applied DC magnetic field increases PQF, or in

another words, reduces the resistance to values near that of air-inductor for higher frequencies.

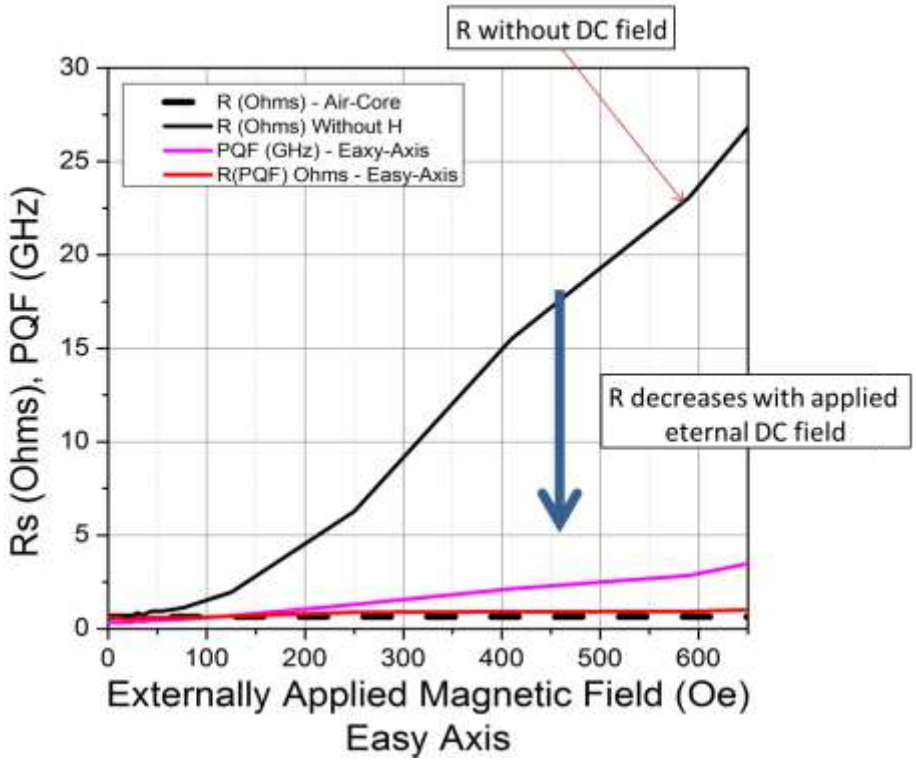

Fig. 6.3: R_s air-core (black/dashed), R_s Baseline Without A Field (black), PQF (pink), and R_s (red) as a Function of H(Easy)

The effect and benefits of introducing an externally applied DC magnetic field on the response of resistance at high frequencies is shown in Fig. 6.3. The figure summarizes the relationship between PQF, QF, and resistance response. The dashed trace is the measured resistance of the air-core inductor. The purple trace is the PQF responses to the applied DC fields. The red trace is the resistance response to the applied field at the corresponding PQF (above it). Finally, the black trace is the resistance response for the magnetic-based inductor at the corresponding PQF, but without an externally applied magnetic field.

In Fig. 6.2, the region for which the resistance response of the magnetic-based inductor is equal to that of its equivalent air-core inductor is the same region as the LFR of Fig. 6.1. The point at which resistance response overcomes the resistance of the air-core inductor is the point at which skin depth and resistance dominates the QF response, and QF begins falling below the PQ value.

An externally applied DC magnetic field increases the skin depth for higher frequencies, therefore suppressing the resistance of the magnetic-based inductor to values equal to that of air-core inductor for larger frequencies. This, in turn, leads to an increase in PQF and PQ. This relationship is reflected in Fig. 6.2, and summarized in Fig. 6.3. As the benefits of the external field clearly show the expansion of the LFR region as the resistance is suppressed for large frequencies due to the presence of external magnetic field. Fig. 6.4 summarizes the enhancement in operating frequency at the PQF value, with the red trace being the FMR, and the magenta trace being the PQF. Fig. 6.5 shows the improvements in PQF and PQ as a result of expanding the LFR region with the externally applied magnetic field.

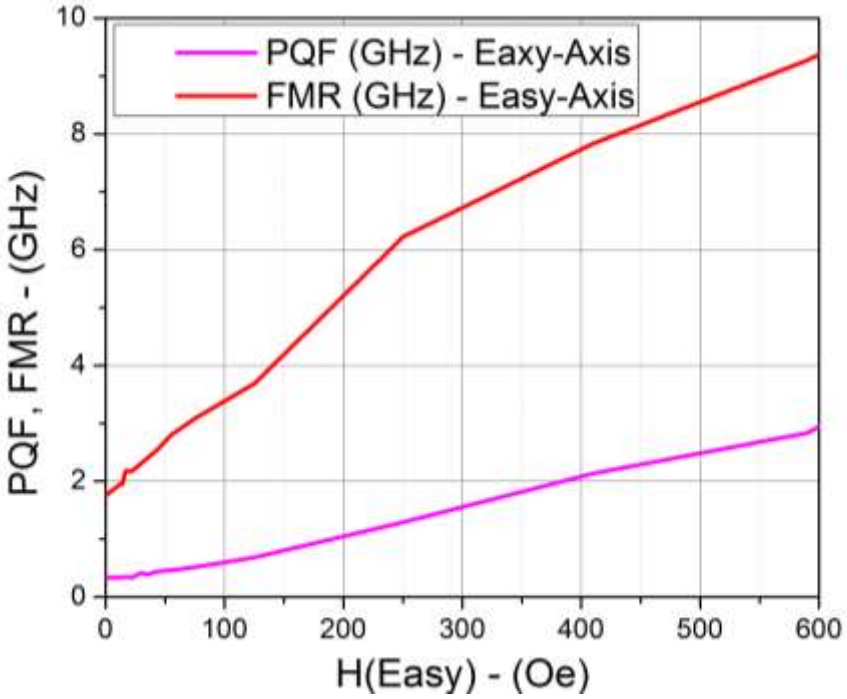

Fig. 6.4: PQF (magenta) and FMR (red) as a Function of H(Easy)

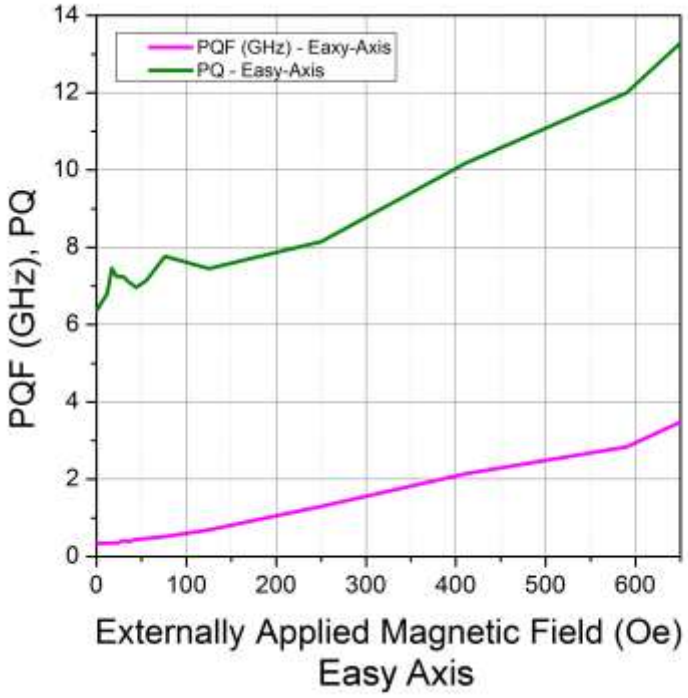

Fig. 6.5: PQF (magenta) and PQ (green) as a Function of H(Easy)

The introduction of an externally applied DC magnetic field along the easy axis of the stripline inductor leads to larger increases in PQF (3.3 GHz for H(Easy) versus 2.2 GHz for H(Hard)) at 650 Oe. For an applied field of 650 Oe, PQF shifted from 0.30 GHz to 3.3 GHz (an 1000% increase—almost twice that of H(Hard) case) , with a PQ increased from 6.2 to 13.5 (118% increase—twice that of H(Hard) case), shown in Fig. 6.1 and Fig. 6.6(b). On the other hand, the inductance decreased from 1.9 nH to 0.65 nH (66%) as shown in Fig. 6.6(a). (H(Hard) decreased by 74% as mentioned before). It is worth noting that in the H(Easy) at 650 Oe inductance did not reach saturation, rather it remained at least 35% above air-core inductance.

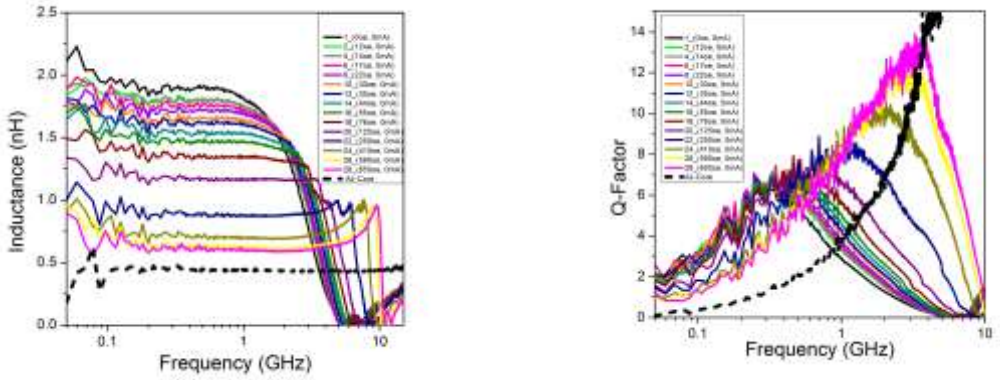

Fig. 6.6: (a) Inductance and (b) QF Response At Various Fields Applied Along The Easy Axis

Table 6.1: Comparison of PQF Shift, Inductance and QF for Differing Field Strengths

H(Hard) Oe	PQF (GHz)	L(nH) at PQF (air-core inductor)	L(nH) at PQF (mag-inductor)	QF at PQF (air-core inductor)	PQ at PQF (mag-inductor)
0	0.30	0.48	1.9	1.3	6.2
590	2.7	0.48	0.66	10	12
650	3.3	0.48	0.65	12.7	13.5

A relatively small increase of an existing strong field (590 Oe to 650 Oe) leads to an insignificant drop in inductance as shown in

Table 6.1 and Fig. 6.6. This translates to a shift from 0.01 nH (0.01%) with inductance value of 0.65 nH (35% above air-core inductance). PQ increases significantly, from 10.0 to 12.7 (27%). When operating near the saturation region, small increases in the applied field lead to significant increases in PQ, and the trend of the QF shows that for very strong fields, PQ of the magnetic-based inductor is converging to the QF of the air-core inductor at the PQF. This conversion is much more pronounced than the H(Hard) case. This indicates that for applied fields at or above the saturation field, the level of PQ becomes that of the QF of air-core inductor. Unlike the H(Hard) case, the inductance does not drop to air-core inductance at 650 Oe. Inductance remains 35% above air-core inductance, whereas for the H(Hard) case, it is only 2% above the air-core inductance. The inductance response to applied magnetic fields was discussed in section 4.1. Future work in understanding the inductance and PQ response for stronger fields, above or near saturation is needed.

As in the case of H(Hard), operating the magnetic-based inductor at frequencies less than the PQF for different fields results in an enhancement of QF and PQ above air-core and magnetic-based inductor without an applied field. The benefits of applying an external magnetic field along the easy axis on the stripline inductor is realized at fields ranging above the threshold value (125 Oe) needed to overcome the shape anisotropy effect, operating below the saturation field. Future studies focusing on applying strong external fields at saturation and beyond should deliver more insight on the QF and inductance response, thereby validating the above analysis.

6.3 Quality Factor Response to DC Magnetic Fields along the Easy Axis

The physics governing the response of QF to an externally applied field along the hard axis, Fig. 6.7, is the same as that for an applied field along the easy axis, section 5.1. The main difference seen at low to moderate fields, when QF response is field-independent due to the domination of shape anisotropy effect. As the externally applied field exceeds the threshold value (125 Oe) that overcomes the shape anisotropy effect, the peak quality factor (PQ) and the PQF increase. For low frequencies (0.3 GHz and below) the quality factor decreases with larger field which is unexpected. Increases in applied field lead to a decrease in permeability which in turn increases the skin depth, as noted in equation 6.1. This subsequently reduces eddy current losses and increases the quality factor. This contradiction between the QF response at low frequencies and equation 6.3 remains an open question.

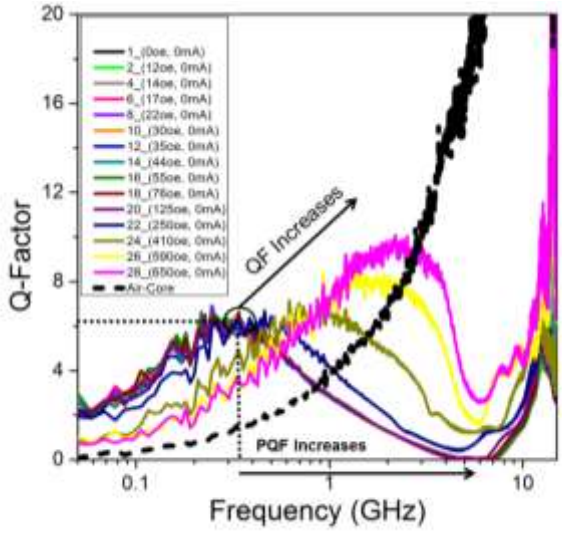

Fig. 6.7: Quality Factor Of Stripline Inductor Device At Various Field Strengths Along The Hard Axis

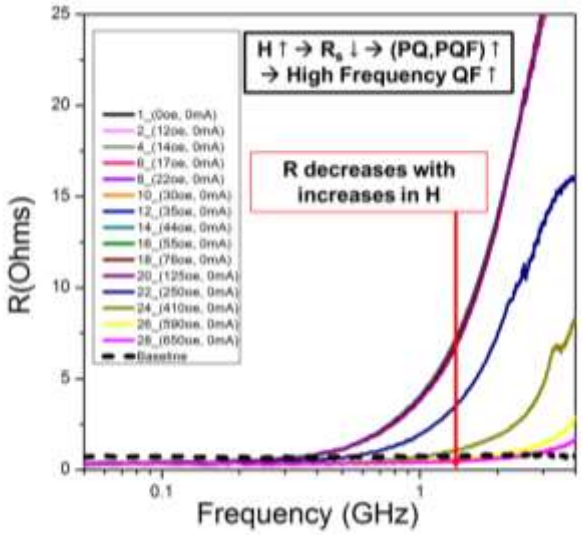

Fig. 6.8: Frequency response of R_s as a Function Of Varying Field Strengths Along The Hard Axis

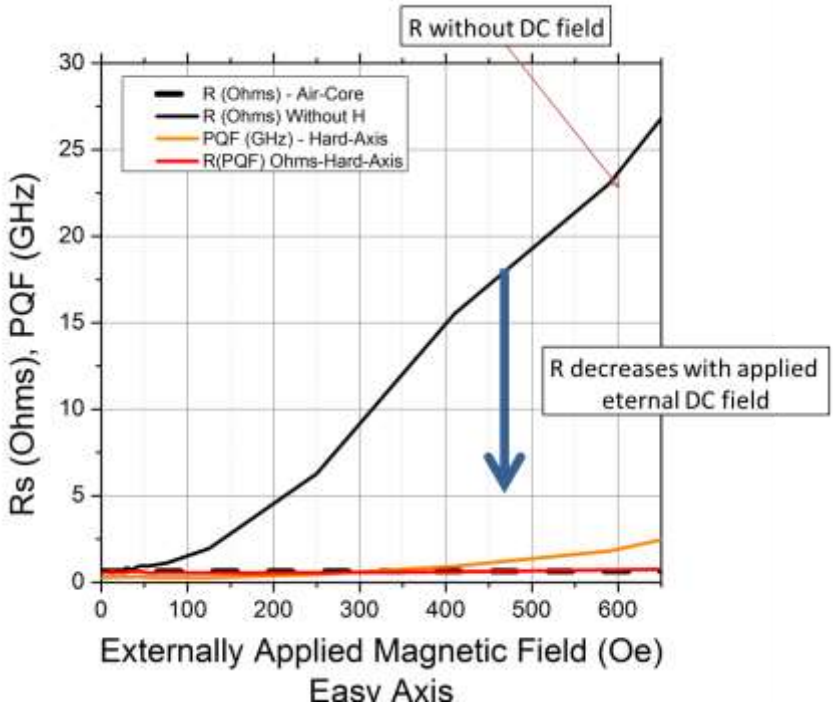

Fig. 6.9: R_s air-core (black/dashed), R_s Baseline Without A Field (black), PQF (pink), and R_s (red) as a Function of H(Hard)

The response of resistance and the effect of applying DC magnetic field along the hard axis of the stripline inductor are reflected in Fig. 6.98 and Fig. 6.109. The details of the physics governing the results along with the analysis can be found in section 6.1. A summary of the enhancement in operating frequency at the PQF value is shown in Fig. 6.911, with the red trace being the FMR and the purple trace being the PQF. Fig. 6.10 shows the improvements in PQF and PQ as a result of expanding the LFR region with the externally applied magnetic field.

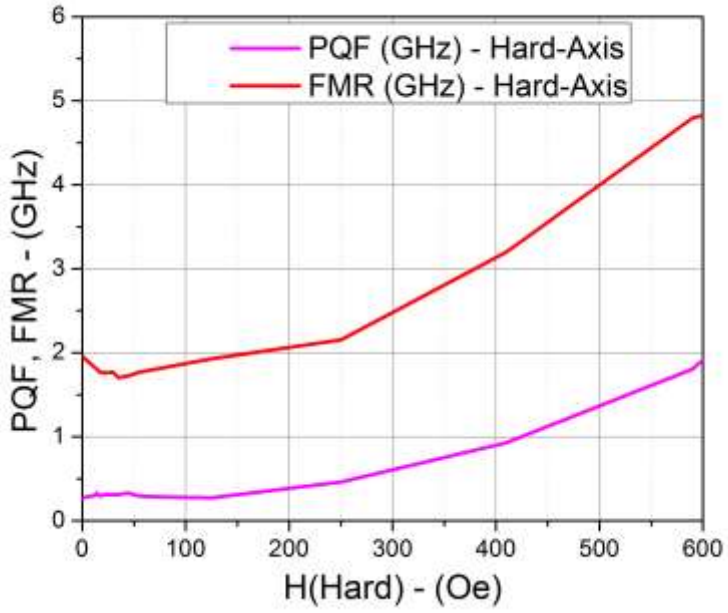

Fig. 6.10: PQF (orange) and FMR (blue) as a Function of H(Hard)

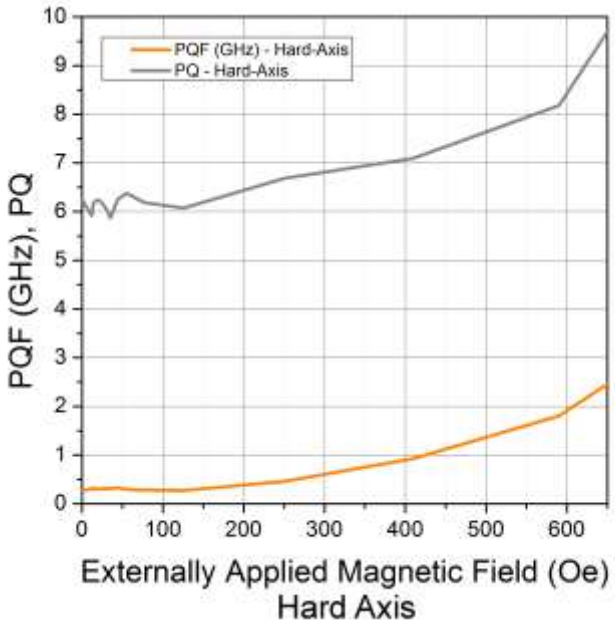

Fig. 6.11: PQF (orange) and PQ (grey) as a Function of H(Hard)

The increase in operating frequency and PQF is substantial. For an applied field of 650 Oe, PQF shifts from 0.30 GHz to 2.20 GHz (633% increase) PQ increased from 6.2 to 9.6 which represents a as shown in Fig. 6.12(b). On the other hand, inductance was found to have decreased by 74% (From 1.9 nH to 0.49 nH) for the same field strength.

Table 6.2: Comparison of PQF Shift, Inductance And QF For Differing Field Strengths

H(Hard) Oe	PQF (GHz)	L(nH) at PQF (air-core inductor)	L(nH) at PQF (mag-inductor)	QF at PQF (air-core inductor)	PQ at PQF (mag-inductor)
0	0.30	0.48	1.9	1.3	6.2
590	1.8	0.48	0.51	6.4	8.1
650	2.2	0.48	0.49	7.5	9.6

Table 6.2 and Fig. 6.12 (a) demonstrate that relatively small increases in field strength for already large applied fields (from 590 Oe to 650 Oe) lead to an insignificant drop (4%) in inductance, with an inductance value of 0.49 nH, which is 0.01 nH above air-core value. But on the other hand, PQ increases significantly, from 8.1 to 9.6 (19% increase). Though small increases in the applied field lead to significant increases in PQ when operating near the saturation region, the trend of the quality factor shows that for very strong fields the PQ of the magnetic-based inductor is converging to the QF of the air-core inductor at the PQF. This indicates that for applied fields at or above the saturation field PQ becomes that of the QF of an air-core inductor at the PQF, just as the case for the inductance parameter. This could warrant future studies of PQ response under fields at and above the saturation field.

(a) (b)

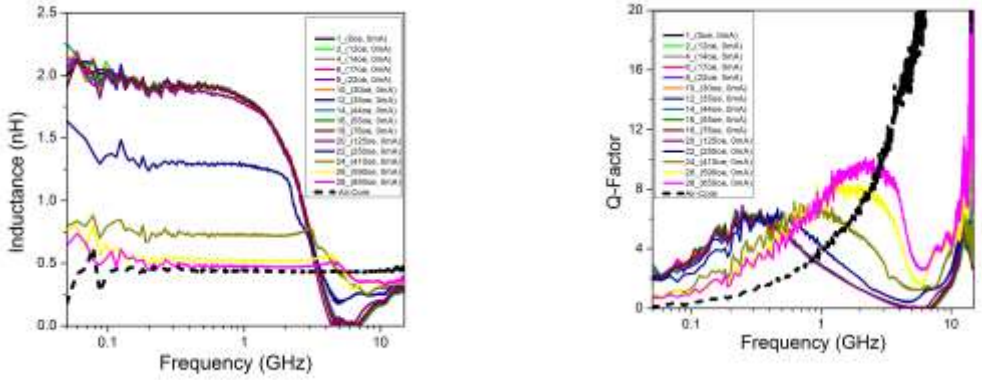

Fig. 6.12: (a) Inductance and (b) QF Response At Various H(Hard) Levels For Stripline Inductors

Even if the target is to drive the inductor to complete saturation, an applied external magnetic field can still be beneficial by operating the inductor at frequencies below the PQF of the saturation state. Such benefits include increases in operating frequency and quality factor. This effect is indicated by the red circle in (b) for which the

QF is 8.8, which is 2.6 units above the PQ without an applied field, and 4.6 units above the QF of an air-core inductor. Furthermore, PQF is at 1.4 GHz, which is a 1.1 GHz increase over the PQF for the case without having an applied magnetic field. Therefore, operating the magnetic-based inductor at frequencies less than the PQF for different applied fields results in QF and PQ enhancements above air-core and magnetic-based inductor without having an applied field, respectively. The benefits of applying an external magnetic field along the hard axis on the stripline inductor is realized at fields ranging above the threshold value needed to overcome the shape anisotropy effect. In this case, that field was measured to be 125 Oe which is below the saturation field. Future studies focusing on applying strong external fields at saturation and beyond should give us more insight and validate the above analysis.

6.4 Quality Factor Response to DC Magnetic Fields along Hard vs. Easy Axes

Applying a DC magnetic field, along the easy or hard axes reduces the resistivity of the inductor's magnetic film. The physics governing the easy and hard axes with respect to resistance and applied DC field is the same. The increase in PQ and PQF for the easy axis is larger than that of the hard axis, as shown in Fig. 6.13. For the same DC magnetic field value, more domains are easily aligned along the easy axis than that of the hard axis. Hence, the axis with easier magnetization is more influence by the DC field and experiences a larger reduction in resistance, which subsequently leads to higher PQ and PQF as seen in Fig. 6.13.

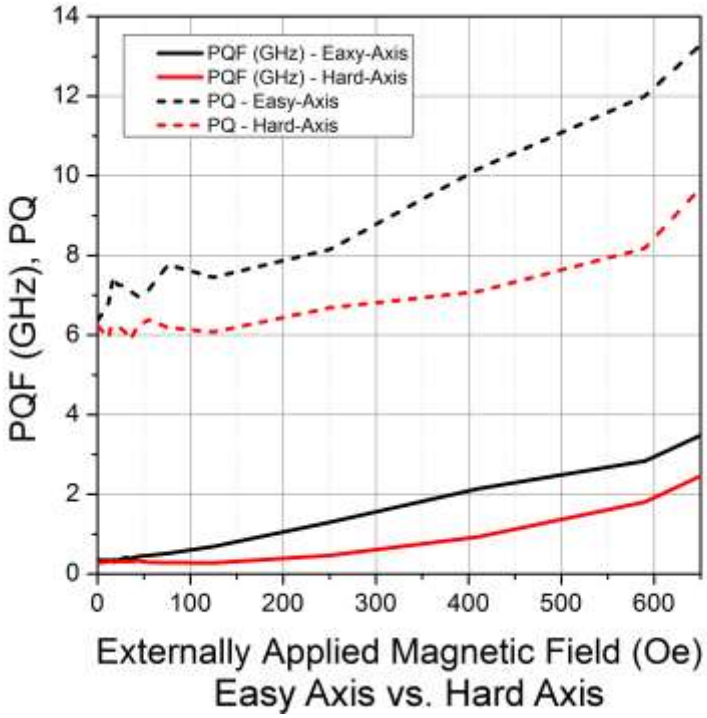

Fig. 6.13: Summary of Quality Factor Response as a function of Applied Magnetic Field

A relationship between the PQF and the resistance response was observed. It is well established that resistance increases with increasing frequency due to the reduction in skin depth, as seen in Fig. 6.14. The frequency at which the resistance response becomes equal to that of the air-core inductor is the PQF frequency as noted in Fig. 6.14. This is true for both H(Easy) and H(Hard) cases. The cross point between the air-core resistance and the magnetic-based resistance is illustrated in Fig. 6.14. For a given on-chip inductor under a certain applied DC field, operating at frequencies with a resistance value below that of the air-core inductor, equates to operating in the frequency dominated (left) region of the QF response, presented in Fig. 6.1 and 6.7. On the other hand, operating at frequencies with resistance above that of the air-core inductor equates to operating at the loss and skin depth-dominated (right) region of the QF response,

presented in Fig. 6.1 and 6.7. The relationship between PQF and the frequency of the resistance cross point is summarized in Fig. 6.15 for both the H(Easy) and H(Hard) cases.

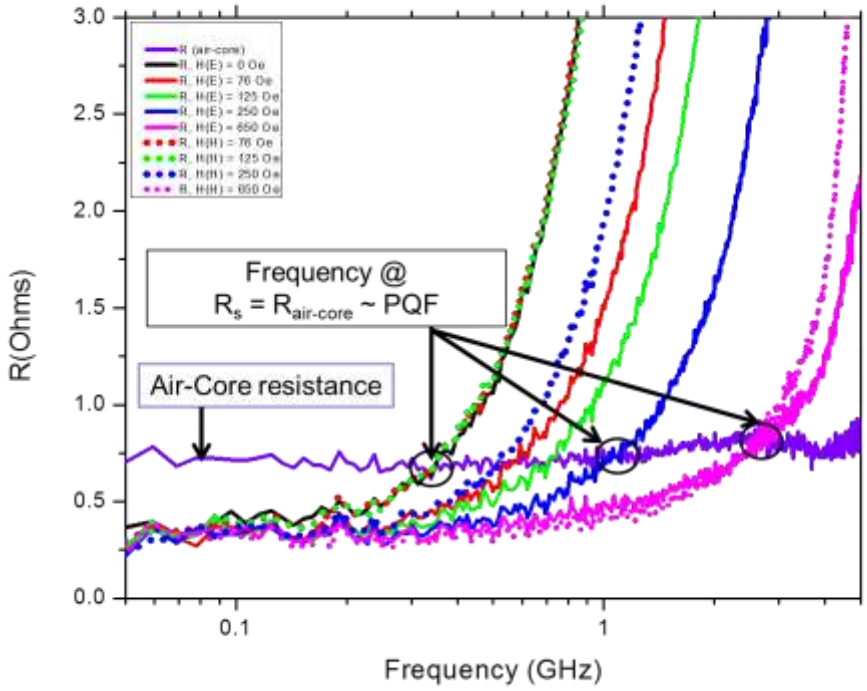

Fig. 6.14: Resistance response compared to air-core resistance for stripline inductors with varying H(Easy) and H(Hard)

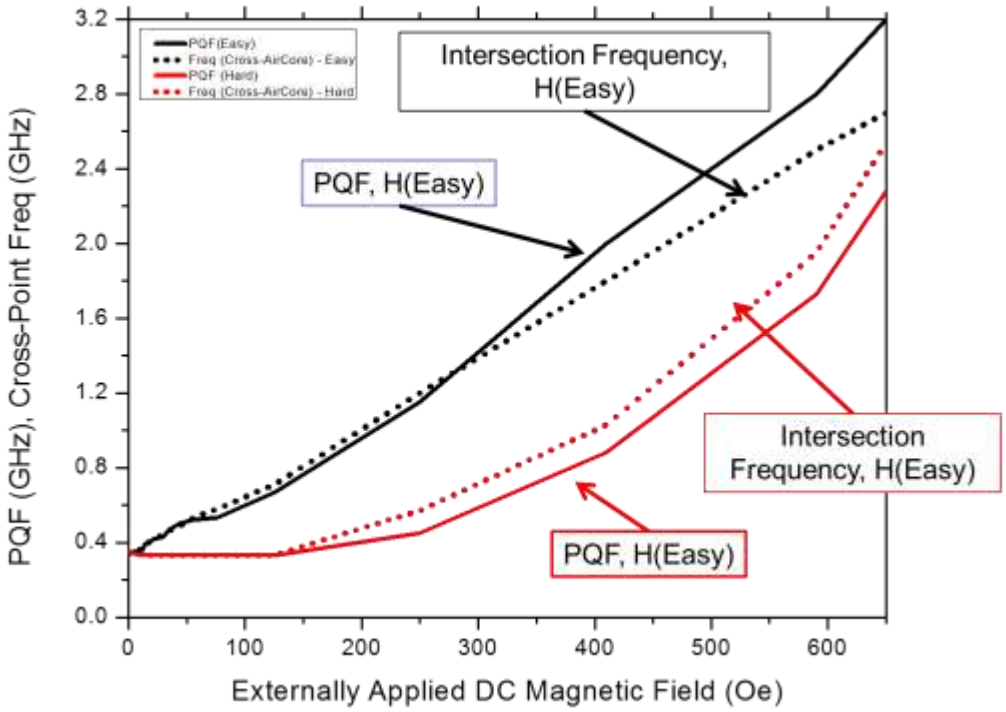

Fig. 6.15: PQF compared to frequency at which the magnetic based resistance response is equal to that of the air-core inductor resistance (Cross-Point Frequency)

Chapter 7

INDUCTOR OPTIMIZATION WITH DC MAGNETIC FIELD

7.1 Parameter Optimization

The characteristics of inductance and QF as a function of an externally applied magnetic field along the easy-axis are shown in Fig. 7.1(a) and Fig. 7.1(b). Operating an inductor at the peak quality factor frequency is the most energy efficient state. An optimization chart for the inductor parameters based on the PQ point was generated utilizing data in Fig. 6.6(a) and Fig. 6.6(b). PQ parameters and their related frequencies were extracted from Fig. 6.6(b), along with extraction of related inductance values from Fig. 6.6(a). The optimization chart value is summarized in Fig. 7.1(a) and the optimization percentage is summarized in Fig. 7.1(b). Externally applied fields with a low value of 12 Oe resulted in optimum conditions of 269% increase in inductance relative to the air-core inductor, a 7% increase in PQ, and a 13% increase in operating frequency. Also externally applied field of 410 Oe resulted in optimum conditions of 56% increase in inductance relative to the air-core inductor, a 68% increase in PQ, and a 545% increase in operating frequency.

(a)

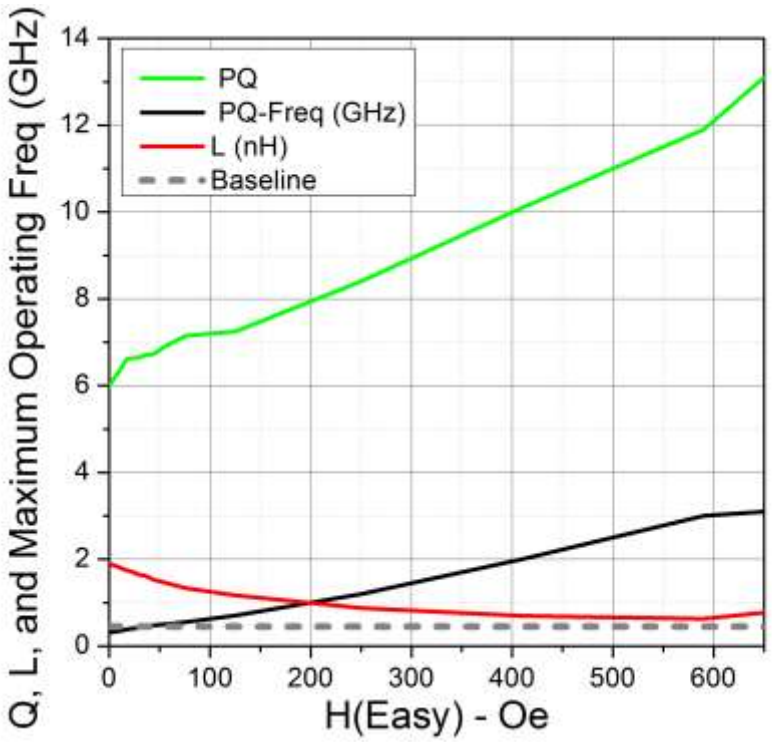

(b)

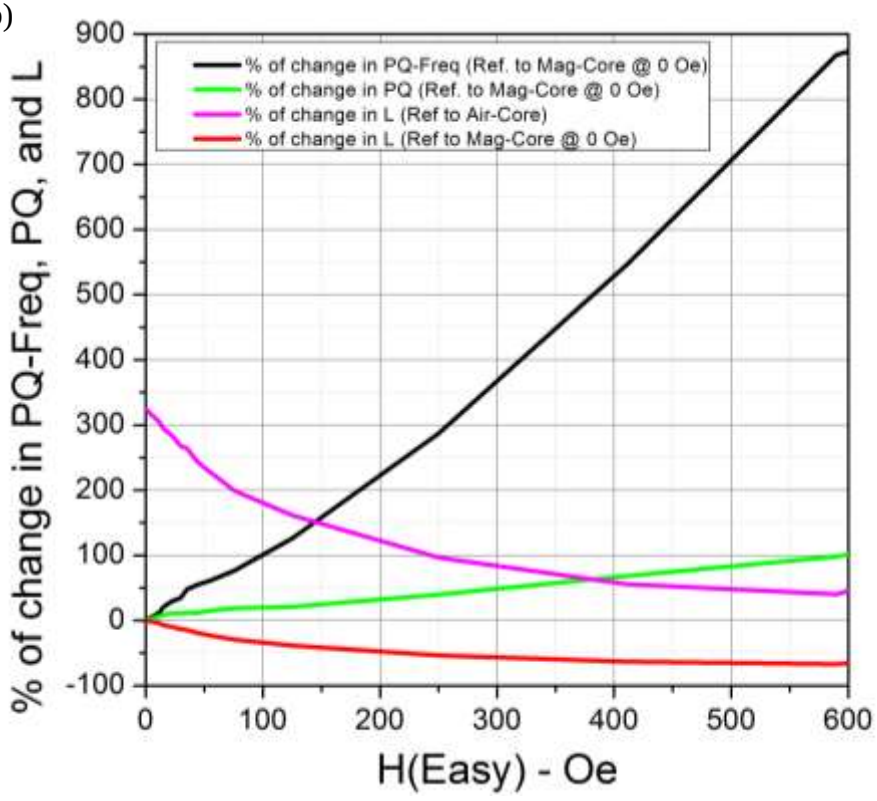

Fig. 7.1: Summary of (a) PQF Shifts and (b) percent change in PQ by Field Strength Along The Easy Axis

For externally applied magnetic fields along the hard axis, data in Fig. 6.12(a) and Fig. 6.12(b) were utilized for the optimization analysis. The optimization charts for this case have been summarized in Fig. 7.2(a), and Fig. 7.2(b), with optimization values and percentage, respectively. Externally applied fields with low value of 410 Oe result in optimum conditions of 61% increase in inductance relative to the air-core inductor, an 8.3% increase in PQ, and a 190% increase in operating frequency.

(a)

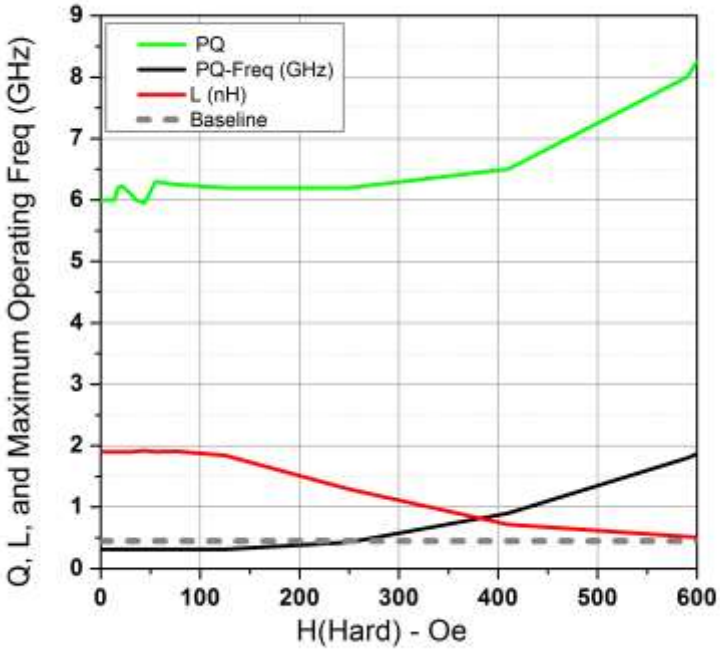

(b)

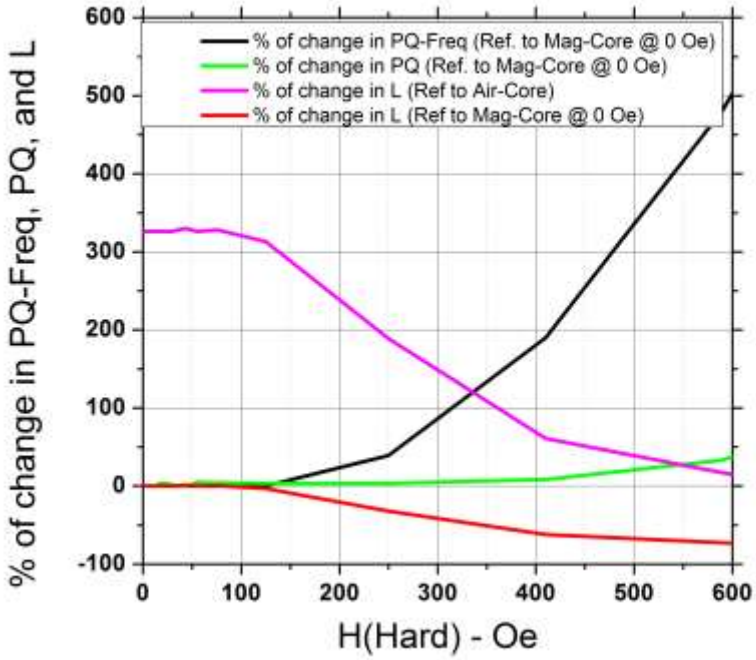

Fig. 7.2: Summary of (a) PQF Shifts and (b) Percent Change in PQ by Field Strength Along The Hard Axis

PQ, operating frequency, and inductance change in various ways with the externally applied magnetic field. Characteristics between the hard axis case and the easy-axis case produce different signatures due to the physical effects of the domains at play. Selecting the required external magnetic field value can be achieved by referring to Fig. 7.3 (a) and (b), and the design criteria based on required inductance or QF can easily be tuned to obtain the optimum characteristics per application of interest.

(a)

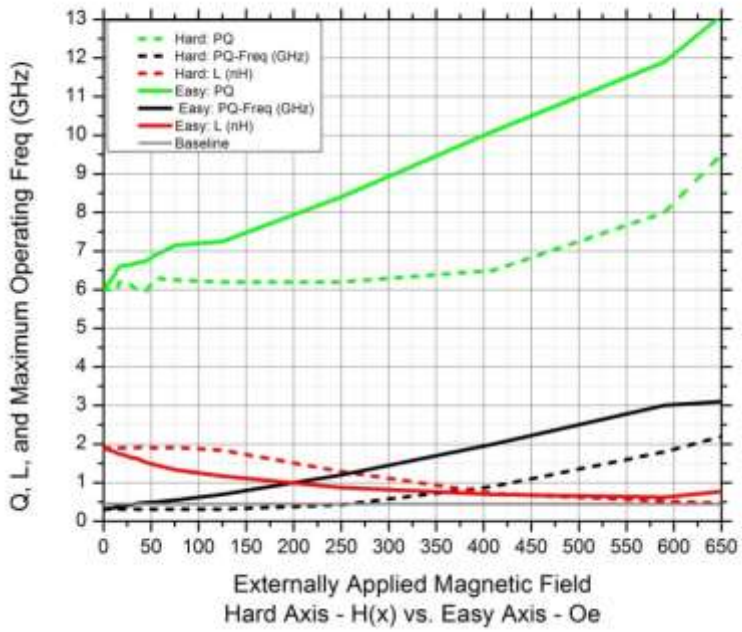

(b)

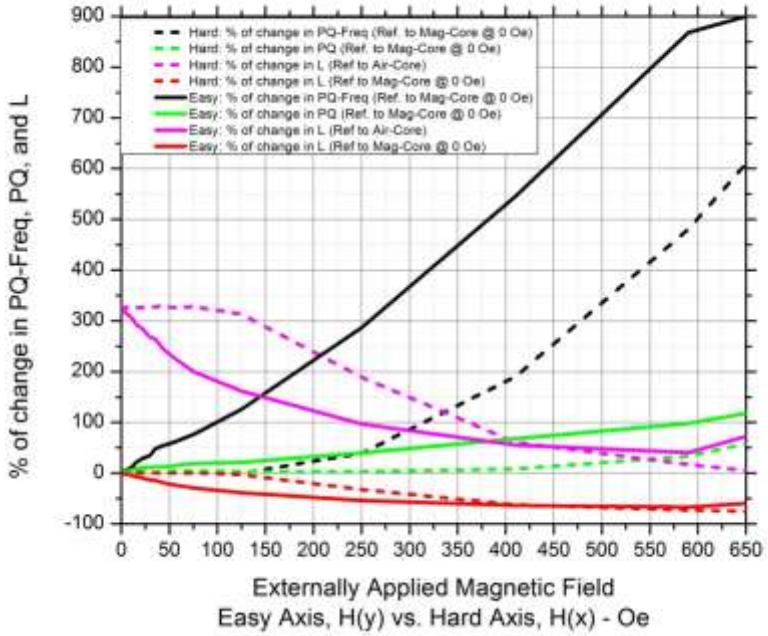

Fig. 7.3: (a)Inductance, QF, and PQF Plotted Together For An External Field Applied Along The Hard And Easy Axis (b) Percent Change Inductance, QF, and PQF Plotted Together For An External Field Applied Along The Hard And Easy Axis

7.2 Conclusion

In this study the effects of an externally applied field on a stripline core, magnetic film on-chip inductor have been explored. The application of the external field in both primary directions has been permuted and the response of inductance, FMR and QF have been measured. In the case of inductance, at a low to moderate applied field along the hard axis, inductance is field independent and this is predominantly due to the shape anisotropy effect. After moving field values from the moderate to high range, the value of inductance drops to about the air core value because the film saturates. At low fields along H(Easy), inductance starts to decrease with higher field. The applied field no longer has to oppose the shape anisotropy effect, and when the field strengths is extended up to the highest range, the inductor still operates at 50% over the air core inductance.

With regards to FMR, the general case is to increase with greater field. However, at low to moderate fields, the inductance level is constant. This is attributed to the shape anisotropy effect which creates field-independent precession. At large enough fields that overcome threshold (125 Oe), FMR apparently continues to increase without bound because the induced field continues to run parallel to the applied field. For applied field in the easy axis, low fields show FMR response increasing, because there is no anisotropy to oppose from the start. FMR continues to increase with larger fields, and this leads to an increase precession frequency. Additionally edge domains are more pronounced in this configuration because the applied field runs along the easy axis, parallel to the stripline.

In the hard axis direction, when low to moderate fields are applied, QF is field independent. However, once again shape anisotropy demonstrates that as the external

field overtakes the threshold field, QF begins to fall. This is viewed as somewhat contradictory to the models that describe eddy current losses through permeability and skin depth effects. PQF also experiences a larger PQF with larger H(Hard) due to decreased permeability but predominately more aligned with FMR operating frequency. For the case of an applied field along the easy axis low to moderate fields instantly see an increase in QF increases. The easy axis case has no shape anisotropy effect to overcome. After a large enough field strength, QF falls, once again for reasons that contradict the model describing permeability with skin depth. Additionally, FMR is also attributed to the shift in PQF. It seems that there is no limit to the shift in PQF because even at 650 Oe, frequency continues to shift as high as 3 GHz.

Chapter 8

SHAPE ANISOTROPY EFFECT AND EXTERNALLY APPLIED DC MAGNETIC FIELD

8.1 Introduction

In this section, the effects of an external DC magnetic field on a spiral inductor, along the easy axis have been explored and analyzed. In section 2.6, the different performance capabilities enabled by a finger shaped via, versus normal vias were investigated. As previously stated, the finger-shaped design performed better because it reduced losses due to eddy currents by miniaturizing as much contact area as possible, and by keeping flux continuous. In section 2.4 the effects of patterning the magnetic films to exploit the shape anisotropy effect were discussed. This plays an enormously important role on inductor characteristics as external DC magnetic field stimulation is introduced to the device. Throughout this study, all unpatterned devices utilize the finger-shaped vias, Fig. 8.1(a).

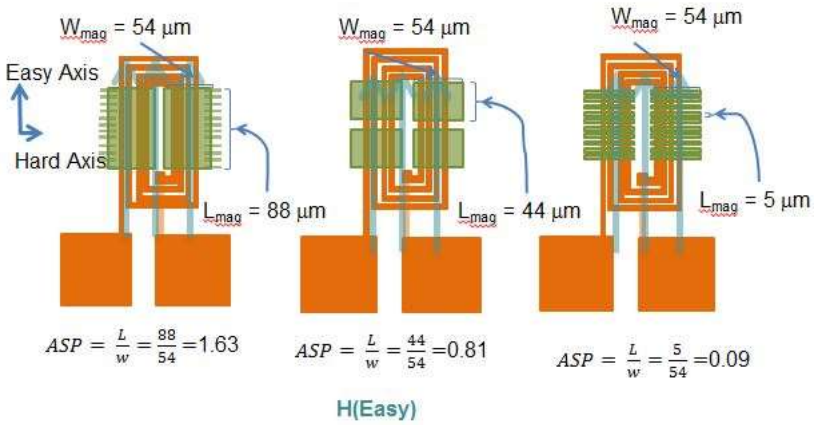

Fig. 8.1: (a) Schematics of Unpatterned, (b) Patterned With 2 Bars, And (c) Patterned With 10 Bars; Spiral Inductors.

8.2 Spiral Inductor Characteristics and DC Magnetic Field along the Easy Axis

The physics governing the inductance response in Spiral inductors is the same that of Stripline inductors, discussed in Chapter 4. Fig. 8.2 is the inductance response of unpatterned spiral inductor under the influnce of and externally applied DC magnetic field along the easy axis.

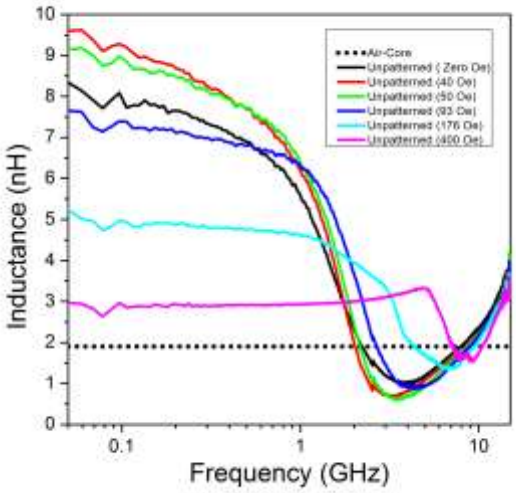

Fig. 8.2: Inductance of 4-turn Spiral Inductor With Complete Co-Zr-Ta-B Film Under Different H Field Biases

The baseline curve for the frequency response of inductance (traced in black) in Fig. 8.2 is established by measuring the magnetic-based inductor without introducing an external magnetic field to the inductor, Fig. 8.1(a). Introducing a weak external DC magnetic field along the easy axis, H(Easy), orients more domains along the easy access. Hence these domains shift from being parallel (or at a slight angle) to the AC current-induced magnetic field, H_{AC}, to become perpendicular to it. This leads to a small increase in the response of these magnetic domains to H_{AC}, and therefore a small increase in susceptibility, and subsequently a small increase in permeability and inductance as it is

reflected for H(Easy) values up to 54 Oe (red line) in Fig. 8.2. This slight inductance increase for low field values along the easy axis is not noted in the strip line inductor. The geometry of the strip line inductor gives an influential shape anisotropy effect, much stronger than that of spiral inductor. The weaker the shape anisotropy effect is, the less are the magnetic domains which that are partially oriented or can be easily oriented along the easy axis.

On the other hand, as the applied magnetic field continues to increase, above 54 Oe, the inductance value across the frequency spectrum begins to decrease. Increases in H(Easy) render magnetic domains less responsive to H_{AC}. This leads to a reduction in susceptibility which subsequently leads to a reduction in permeability and inductance as it is reflected in Fig. 8.2 fields above 54 Oe. Further increases in the applied field exert stronger forces on the magnetic domains, hence hindering their response to the AC current-induced magnetic field, H_{AC} which leads to further decreases in susceptibility and subsequently further decreases in permeability and inductance (Fig. 8.2). At very large fields near saturation, the majority of magnetic domains (except the edge domains) are in parallel to the easy axis and being influenced with the strong force exerted by the large fields. At very large H(Easy) values the magnetic domains (except edge domains) become completely dominated by H(Easy), that is they become non-responsive to H_{AC}. Hence, the susceptibility drops reflecting the susceptibility of edge domains to H_{AC}. This is the point at which the film becomes fully saturated along the easy axis and the inductance value becomes very close to that of air-inductor. This is further noted in the magenta trace of Fig. 8.2, where the inductance value at an applied field of 400 Oe is 3 nH, which is 50% above that of air-core inductor.

(a) (b)

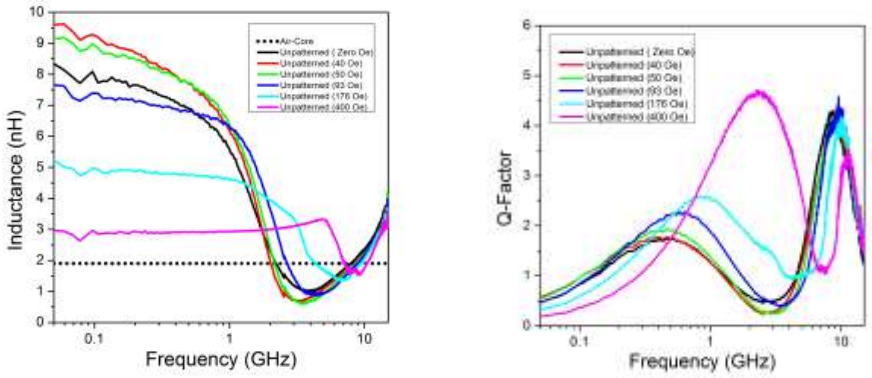

Fig. 8.3: (a) Inductance and (b) Quality Factor responses for a Spiral Inductor with Unpatterned CZTB Film

The above analysis is reflected in the data of inductance (Fig. 8.3 a) and QF (Fig. 8.3 b). At high external field strengths, the inductance value drops across the spectrum close to the values of the air-core inductor. Because when magnetic domains (magnetization) in the film are subject to high fields, they become unresponsive to the induced AC current-induced magnetic field, H_{AC} which points perpendicular to it. On the other hand, an increase in PQ and PQF of spiral inductors is observed and is discussed in the subsequent section.

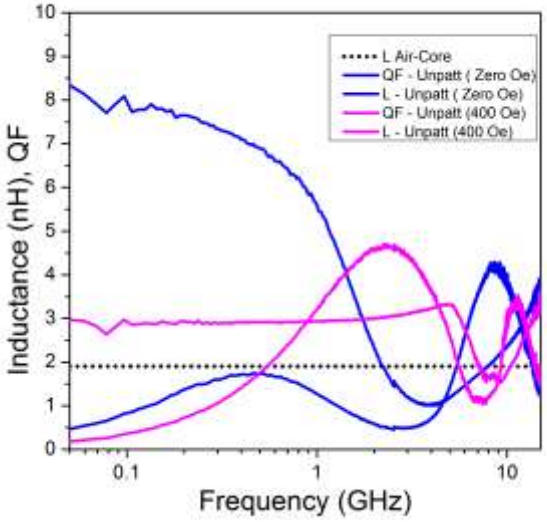

Fig. 8.4: Effect of Externally Applied Field on Inductance, QF, PQ, and PQF Responses For Unpatterned Spiral Inductor

A peak quality factor, PQ, of 4.6 at PQF of 2.0 GHz was achieved for an applied DC field of 400 Oe. This represents a 156% increase in PQ with a shift in PQF from 0.4 GHz to 2.0 GHz, a 400% increase in PQF (Fig. 8.4). This improvement in PQ and PQF comes at the expense of the inductance with a 58% decrease in inductance detected for an applied field of 400 Oe, Fig. 8.4, and Table 8.1. However, despite the decrease in inductance values, inductance remained at least 50% above air-core inductors. In the low frequency region (frequencies below the PQF) the quality factor decreases with larger applied field. This is not expected because the increase in the applied fields leads to the decreases in permeability, thereby leading to increases in skin depth, according to equation 6.1. This subsequently reduces eddy current losses and increases the QF. This contradiction between the QF response at low frequencies and equation 4.1 remains an open question, just as in the case for strip line inductor.

Table 8.1: Relative Shifts in PQF, Inductance, and QF at Associated Applied Fields

H(Hard) Oe	PQF (GHz)	L(nH) at PQF (air-core inductor)	L(nH) at PQF (mag-inductor)	QF at PQF (air-core inductor)	PQ at PQF (mag-inductor)
0	0.40	1.9	7.2	0.5	1.888
400	2.2	1.9	3.0	1.7	4.666

8.3 Spiral Inductor Characteristics and Shape Anisotropy Effect

The patterned magnetic films were used in order to explore the shape anisotropy effect on the response of the inductor. As previously described, patterned films (Fig. 8.1(b), Fig. 8.1(c), Fig. 8.4, Fig. 8.8) were composed of magnetic bars at varying lengths, thereby modulating the device aspect ratio. For the purpose of this study, the device aspect ratio is defined as the length along the hard axis, divided by the width along the easy axis. Differences in aspect ratio were varied with the unpatterned film being one extreme condition, and the 10 Bars patterned film being the other extreme condition. At pattern density, 2 bars, the reduction in inductance (red trace in Fig. 8.5) is due to the loss in magnetic material that is introduced by patterning the film. On the other hand, as the film takes on a higher pattern density (and thus smaller aspect ratio), it is found that the influence of shape anisotropy effect becomes the dominant one, leading to a significant reduction in inductance, as seen by the blue trace in Fig. 8.5.

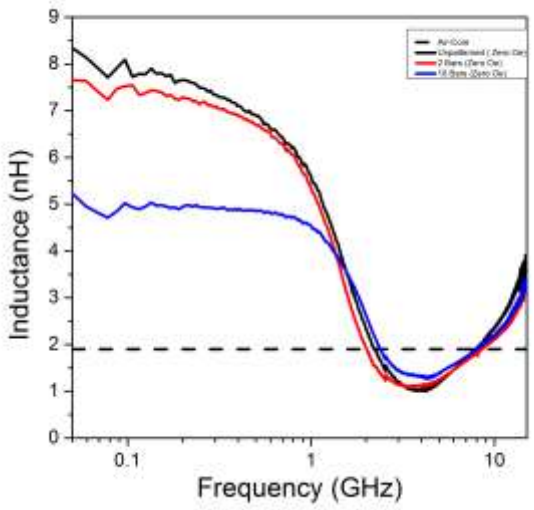

Fig. 8.5: Inductance Response To Patterning and Shape Anisotropy Effect

Furthermore, a slight increase in PQ and PQF is induced by influence of shape anisotropy effect, as seen in Fig. 8.6. This high frequency QF enhancement comes from the reduction in resistance at higher frequency, as seen in Fig. 8.7.

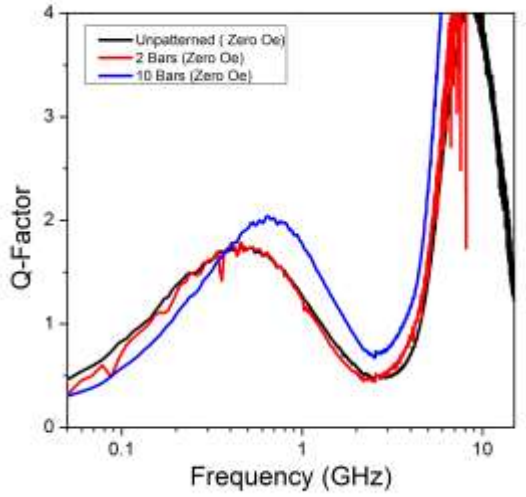

Fig. 8.6: QF Response To Shape Anisotropy Effect

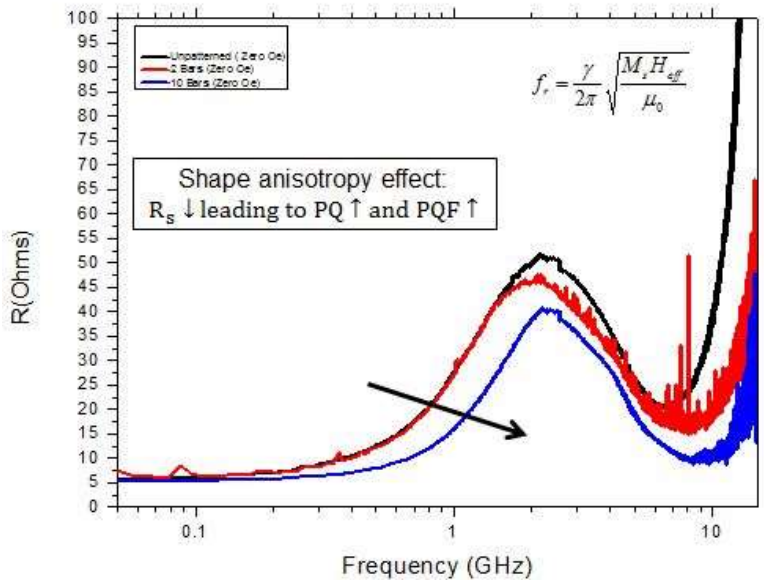

Fig. 8.7: QF Response To Shape Anisotropy Effect

8.4 Inductance Response to DC Magnetic Field and Shape Anisotropy Effect

The patterned magnetic films were used in order to explore geometric considerations on the saturation field. As previously described, patterned films were composed of magnetic bars at varying lengths, thereby modulating the device aspect ratio. Differences in aspect ratio were varied with the unpatterned film being one extreme condition, and the 10 Bars patterned film being the other extreme condition(Fig. 8.8). As the films take on a higher pattern density (and thus smaller aspect ratio), it is found that the effect of an applied external magnetic field along the easy axis becomes progressively negligible, as seen in the extreme case of Fig. 8.9.

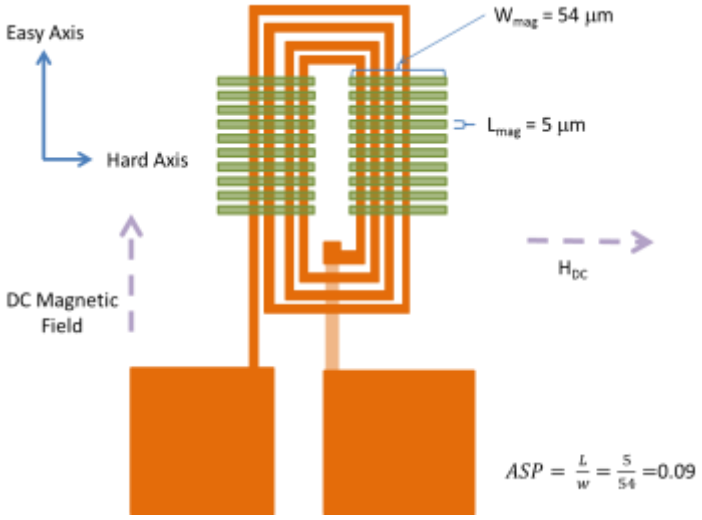

Fig. 8.8: Schematic of Spiral Inductor with Patterned CZTB films of Varying Aspect Ratios (length/width)

In section 2.3, the importance of shape anisotropy in the context of these measurements was discussed. The shape anisotropy effect comes into play as the aspect ratio decreases to the point that the easy and hard axes become revered. The relative magnitude of this effect can be modulated by the level of aspect ratio itself. For example, in Fig. 8.9 at zero fields, inductance actually drops below the state without an externally applied field. As it was discussed in section 8.2, the initial drop (for 2 bars) is attributed to the fact that the amount of magnetic material has reduced, where the large drop for the 10 bars case is due to the domination of shape anisotropy effect.

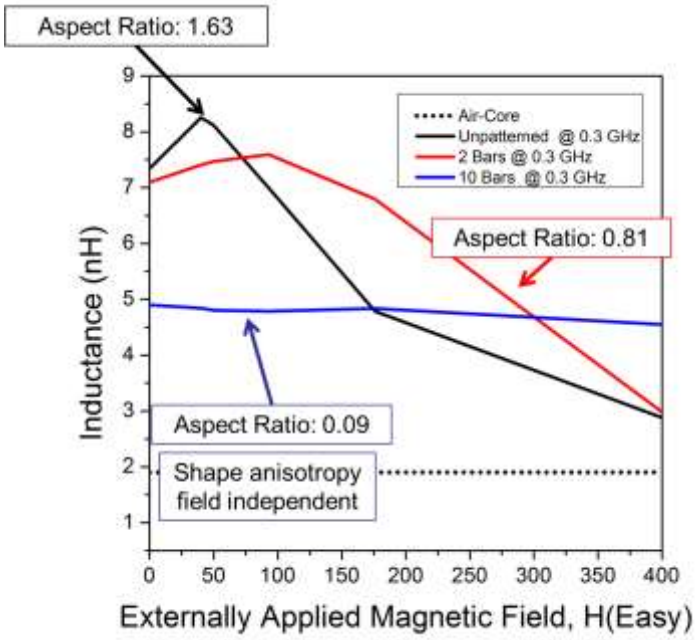

Fig. 8.9: Inductance Response of Spiral Inductor to Shape Anisotropy Effect with H(Easy)

The unpatterned case and low densely patterned film (2 bars) experience a very small influence of shape anisotropy effect due to the largest aspect ratio. As the transition from unpatterned film to more dense patterned films is undertaken, the shape anisotropy effect becomes more pronounced to the point that the easy and hard axis exchange with one another (the 10 bars case). In this state, the externally applied field has almost no influence on the response of the magnetic domains to H_{AC}. Hence, the film's susceptibility and inductance responds independently to the external field, as seen in Fig. 8.9.

The transition from unpatterned film to densely patterned films results in a reduction of the influence of applied field and an increase in the influence of shape anisotropy effect until the shape anisotropy effect becomes the dominant one (Fig. 8.10).

Hence, utilizing inductors with densely patterned magnetic films leads to a magnetic field independent inductance response. This is desirable for commercial applications.

8.5 Quality Factor Response to DC Magnetic Field and Shape Anisotropy Effect

The trend in QF response to the externally applied DC magnetic field for spiral inductor is the same as that for the inductance response, section 8.3. Fig. 8.10 shows the response of the QF to the externally applied magnetic field along the easy axis of spiral inductors with different aspect ratios. For densely patterned film the shape anisotropy becomes the dominant effect (blue trace in Fig. 8.10 and Fig. 8.11) and the response of the QF (Fig. 8.10) and resistance (Fig. 8.11) becomes independent of the externally applied DC magnetic field. The physics governing this behavior is discussed in section 8.3.

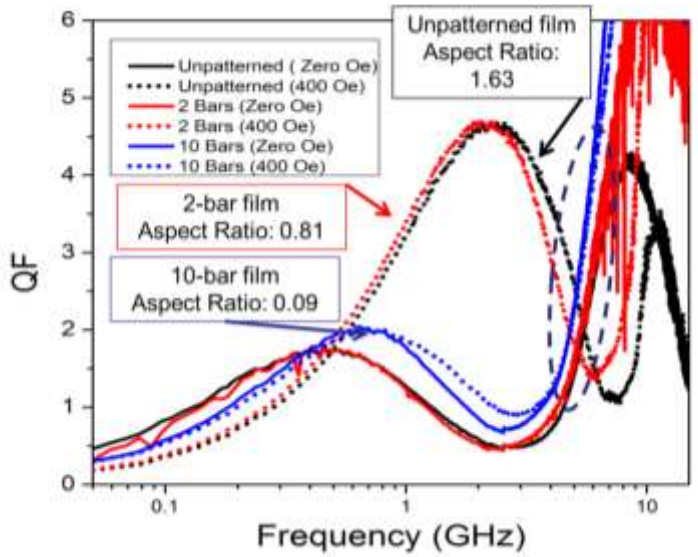

Fig. 8.10: Quality Factor Response of Spiral Inductor to Shape Anisotropy Effect with H(Easy)

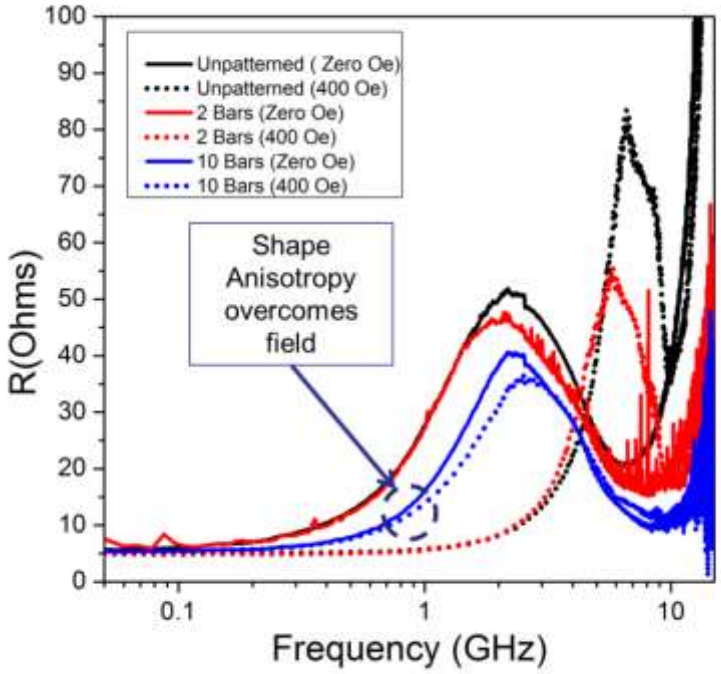

Fig. 8.11: Resistance Response of Spiral Inductor to Shape Anisotropy Effect with H(Easy)

Chapter 9

EFFECT OF CURRENT-INDUCED MAGNETIC FIELD ON ON-CHIP INDUCTORS

9.1 Introduction

DC current (I_{dc}) was introduced to study the effect of operating current on inductor's electrical characterization during and after operation. The DC current was also introduced to examine the inductor's current carrying capability experimentally. The RF signal was superimposed on the DC current via the bias-tea as it was discussed in the experimental setup (Fig. 4.3). The current induced magnetic field ($H_{DC/AC}$) increases with increases in the operating current. The plane of this current induced magnetic field is perpendicular to the current flow and parallel to the hard axis. Hence, this current induced magnetic field resembles the case of an externally applied magnetic field along the hard axis (section 3.1). Though $H_{DC/AC}$ resembles H(Hard), the trends in their effect on the inductor's electrical characterization is different. This difference could stem from the natural difference in the shape and nature of the current induced magnetic field. The current induced magnetic field is in a circular plane that is perpendicular to the current flow but the DC magnetic field is applied in parallel to the surface of the inductor or film. Furthermore, the copper wire is located in the center of the magnetic film. This leads to an even distribution of $H_{DC/AC}$ on both sides of the magnetic film. On the other hand, the strength of the DC magnetic field does not reflect an even distribution to both sides of the magnetic film (to the right, and to the left of the copper wire).

9.2 Inductor Characteristics and Current-Induced Magnetic Field

An increase in the strength of the operating current leads to a reductions in inductance (Fig. 9.1). The physics governing this reduction is that of the same discussed H(Hard) case (section 4.2). The trends in inductance response is the same as in the H(Hard) case. On the other hand, FMR trends are different (Fig. 10.1, Fig. 10.2). FMR initially increases with increases in current-induced magnetic field $H_{DC/AC}$, just as for the H(Hard) case. But at some point, FMR starts to decrease with increases in $H_{DC/AC}$ (or current), unlike the case of the H(Hard) were FMR continues to increase with externally applied field (Fig. 4.2).

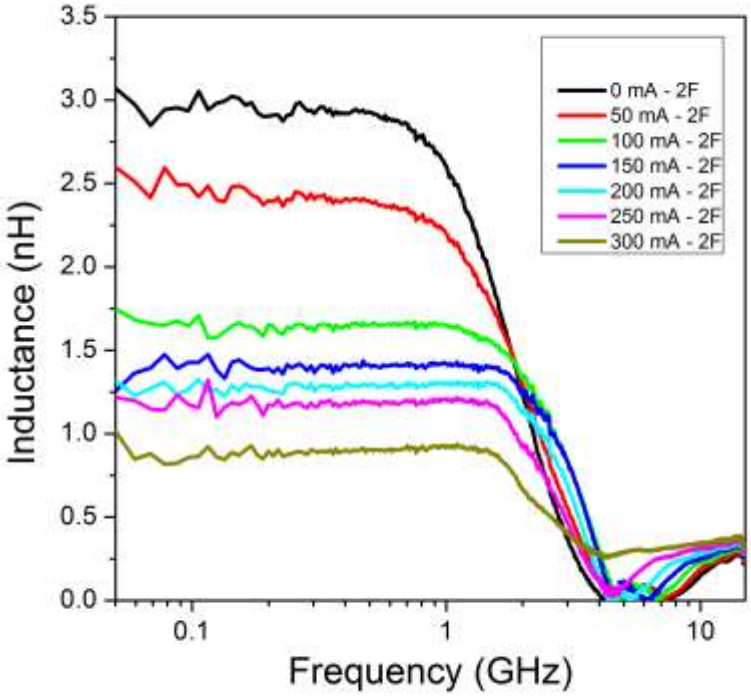

Fig. 9.1: Inductance Response to Current-Induced Magnetic Field (DC Current)

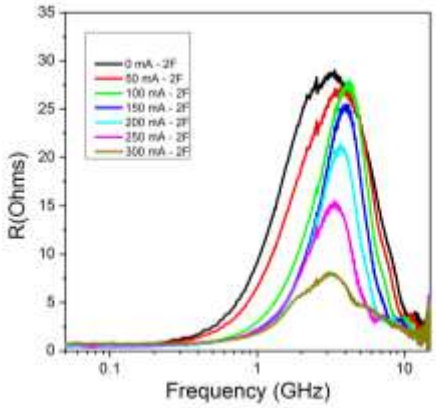

Fig. 9.2: Resistance Response to Current-Induced Magnetic Field (DC Current)

Fig. 9.3 represents the main obstacle that is hindering magnetic-based on-chip inductors from becoming a practical solution to the monolithic system on chip quest. Two stripline inductors- one with continuous film, the other is an identical inductor but with a 30 bars patterned film were characterized. Inductance decreases with increases in the operating current, for both inductors (Fig. 9.3). The physics behind this response is detailed in Chapter 5.

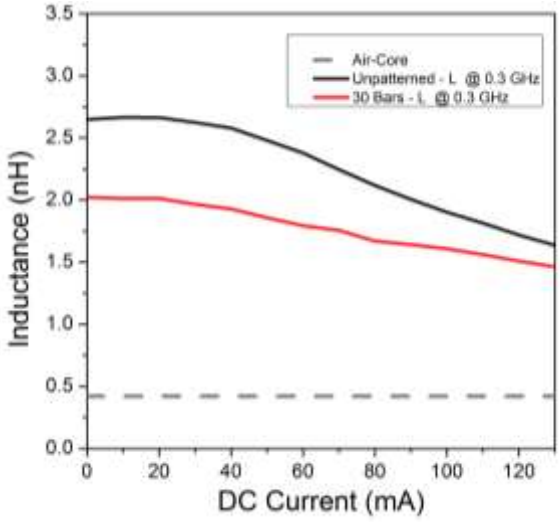

Fig. 9.3: Inductance Response to Operating Current with and without Patterned Magnetic Film

The quality factor response for an externally applied magnetic field was discussed in details in chapter 6. Quality factor initially increases with the increase in current-induced magnetic field $H_{DC/AC}$, just as in the case for the externally applied magnetic field (Fig. 9.4). But at some point QF starts to decrease with the increase in $H_{DC/AC}$ (or current), unlike the case of the externally magnetic field where QF continues to increase with increases in the externally applied field (Fig. 6.7). This shift in trend of increasing QF value stems from a shift in the resistance trends (Fig. 9.5). The resistance starts out by decreases with the increase in $H_{DC/AC}$ (or current), but at some point the resistance starts to increase for larger $H_{DC/AC}$ (or current). This change in resistance behavior and the physics governing it is not well established yet.

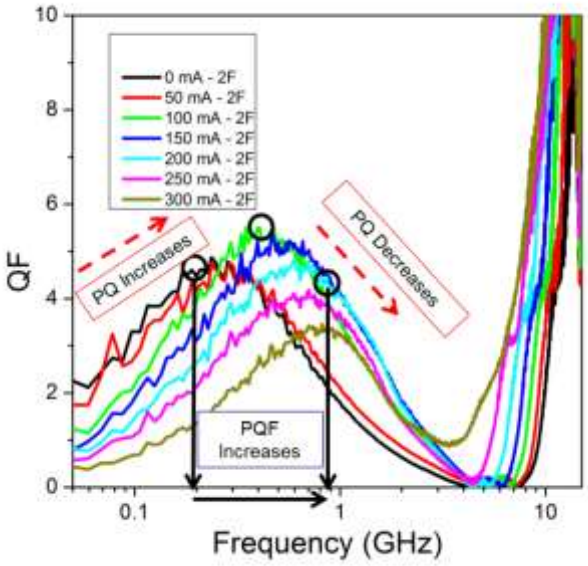

Fig. 9.4: Quality Factor Response to Current-Induced Magnetic Field (DC Current)

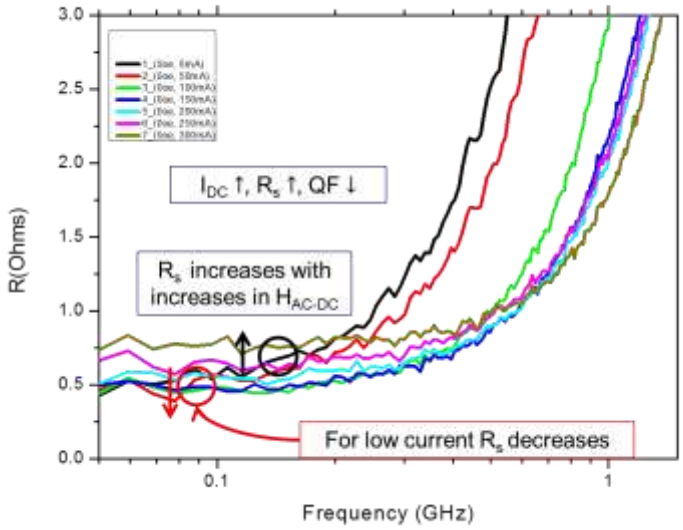

Fig. 9.5: Low Frequency Resistance Response to Current-Induced Magnetic Field (DC Current)

9.3 Inductor Degradation and Current-Induced Magnetic Field

Degradation study is the study of the changes in the inductor characteristics due to the electrical stress of the operating current. In another word, this is the study of the changes in magnetic domains due to the stress of the current-induced magnetic field. To examine the degradation experimentally, a stripline inductor was exposed to an electrical stress of operating currents of 0 mA, 50 mA, 100 mA, 150 mA, 200 mA, 250 mA, and 300 mA. Then a DC current independent inductance response was measured (red trace in Fig. 9.6). The same electrical stress was re-conducted on the same device and once again the DC current independent inductance response was measured (red trace in Fig. 9.7). The difference between the inductance state before the electrical stress (black trace in Fig. 9.7) and the inductance state after the electrical stress (red trace in Fig. 9.7) is a representation of inductance degradation.

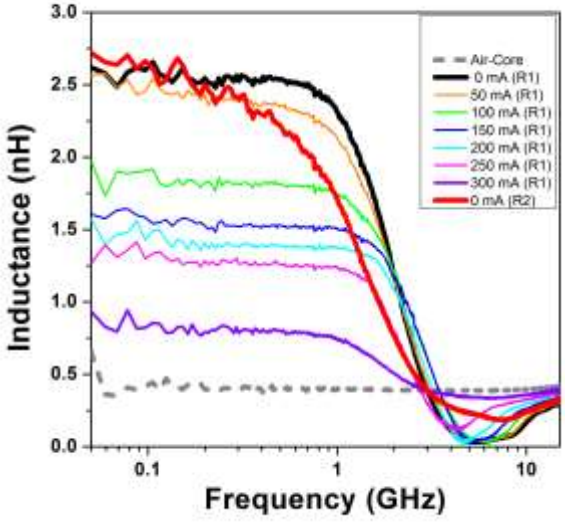

Fig. 9.6: Inductance Degradation Observation and Electrical Stress (Initial Trial)

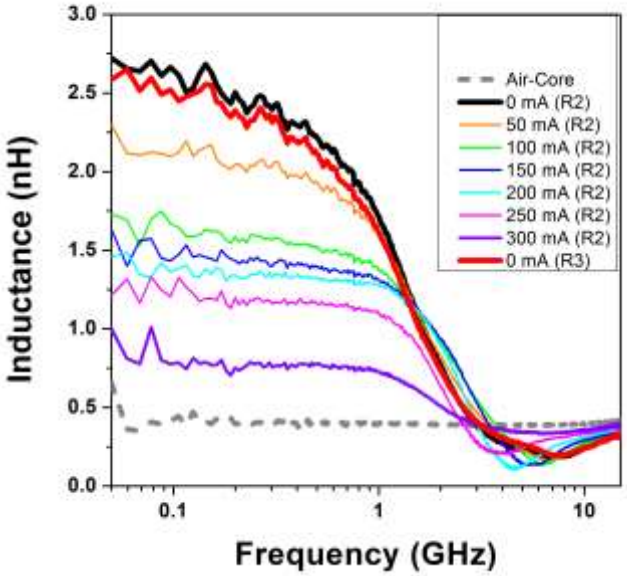

Fig. 9.7: Inductance Degradation Observation and Electrical Stress (Second Trial)

The electrical stress of 0 mA, 50 mA, 100 mA, 150 mA, 200 mA, 250 mA, and 300 mA was conducted in five cycles on the device. The DC current independent

inductance response was measured between each cycle and is summarized in Fig. 9.8. The degradation in inductance due to electrical stress is summarized in Fig. 9.8. Stress cycle number five (red trace in Fig. 9.8) has the maximum degradation as expected because it is the cycle that experienced the most stress for it being the last stress cycle. The quality factor response for the fifth cycle of electrical stress is presented in Fig. 9.9. There is a small degradation in QF in the low frequency region.

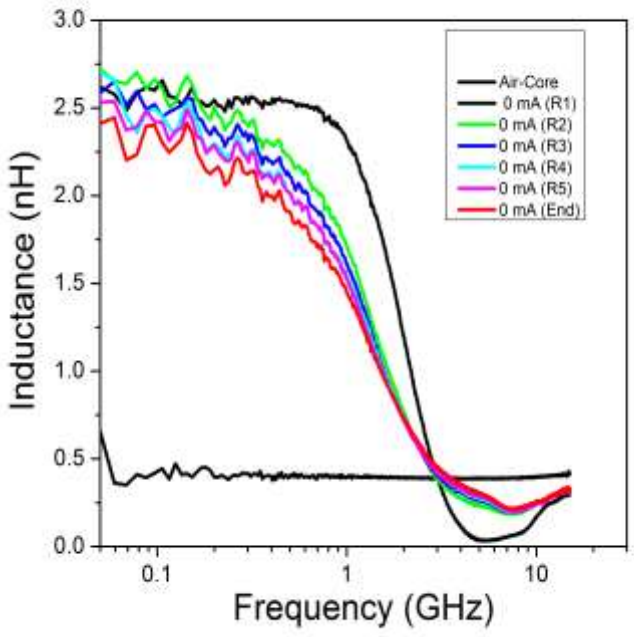

Fig. 9.8: Inductance Degradation due to Electrical Stress

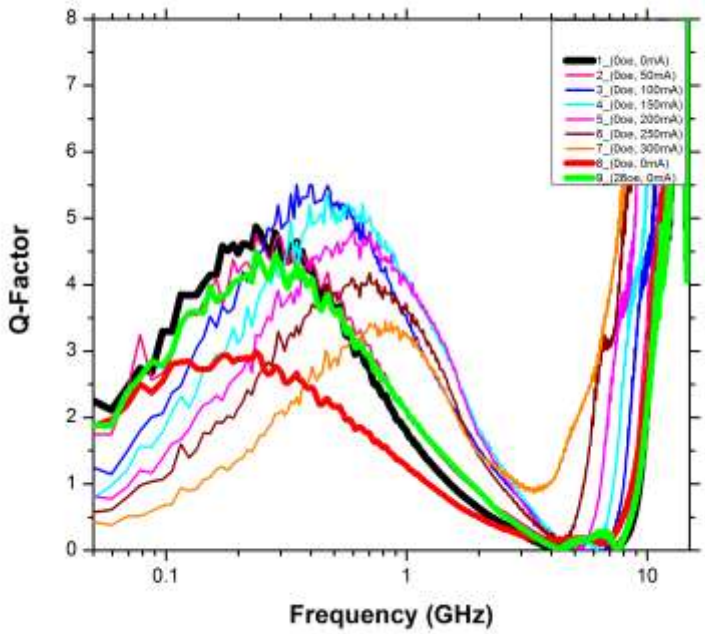

Fig. 9.9: Quality Factor Degradation (red trace) due to Electrical Stress. Green Trace is Degradation Remedy due to DC Magnetic Field

9.4 DC Magnetic Field as a Solution to Inductor Degradation

As discussed in section 9.2, degradation is attributed to the inherent stress of the current induced magnetic field and its influence on magnetic domains. To encounter this stress, a small external DC magnetic field was applied along the easy axis. The externally applied field overcomes the current-induced magnetic field and becomes the determining factor of the stability of magnetic domains, and hence inductor characteristics. Fig. 9.11 (a) shows the inductance characteristics after it has gone through an electrical stress without having the externally applied DC magnetic field. The difference in the initial and final conditions due to degradation is clearly marked in the dotted black trace in Fig. 9.11(a). On the other hand, the same electrical stress was conducted but with a DC

magnetic field of 57 Oe. There was no difference in inductance response between the initial and final states due to the presence of the external DC magnetic field, as it is shown in the dotted black trace in Fig. 9.10(b). The quality factor degrades with electrical stress as seen in Fig. 9.9 and Fig. 9.11(a). The degradation in quality factor can also be overcome by utilizing a DC external magnetic field (9.10(b), Fig. 9.11(b), and Fig. 9.9). Increases in the strength of the DC magnetic field enhances the anti-degradation remedy as seen in Fig. 9.10(b) and 9.11(b)

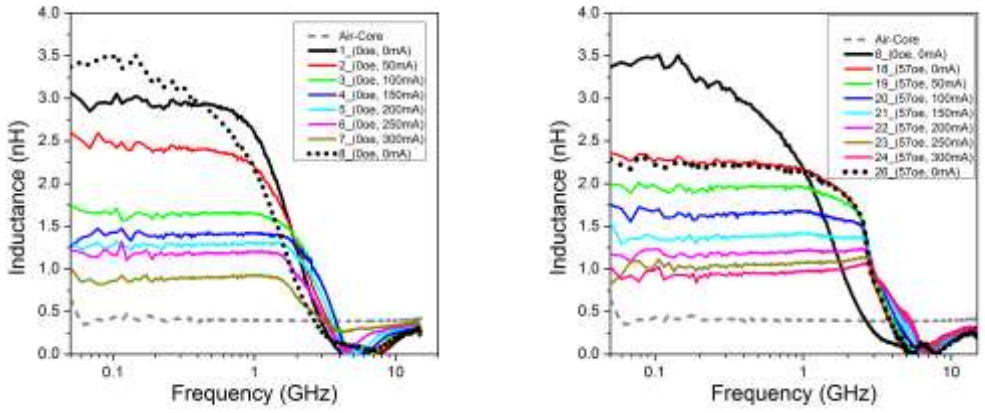

Fig. 9.10: (a) Inductance Degradation (b) Degradation Remedy Utilizing External DC Magnetic Field

(a) (b)

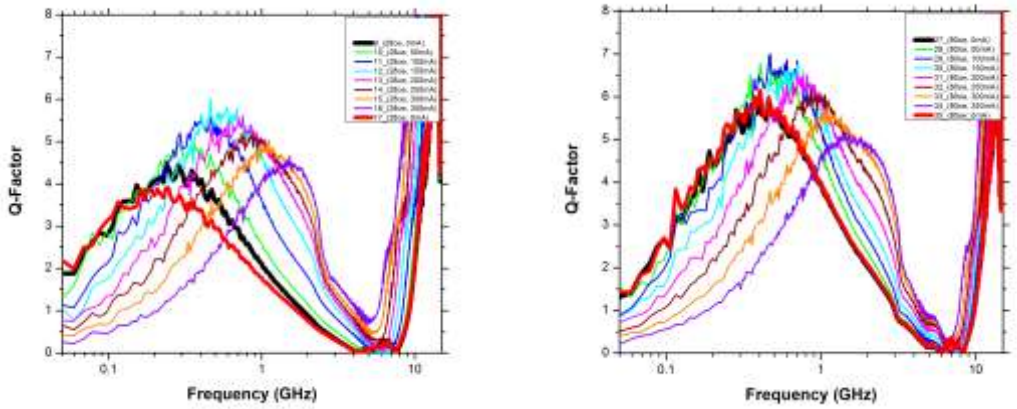

Fig. 9.11 Quality Factor Remedy for (a) Low DC Magnetic Field (b) Large DC Magnetic Field

Detailed future study of inductor degradation is needed. Accelerated life test, and time based degradation with and without electrical stress is needed. Preforming physical characterization (domain imaging) in parallel to the electrical characterization and stresses should give a comprehensive picture of the degradation mechanism and the best way to overcome it. This brief study sheds some light on the degradation topic and concludes of applying a permanent DC magnetic field of small value along the easy axis of the magnetic-based on-chip inductor as a remedy to the degradation issue, during and after operation.

Chapter 10

CURRENT CARRYING CAPABILITY

10.1 Introduction

In this chapter the effect of externally applied DC magnetic field on current carrying capability or saturation current (I_{sat}) was experimentally examined. Fig. 10.1 shows the schematic representation of the H-B plot with the saturation current of the inductor donated by the green arrow. The idea for applying the external DC magnetic field along the easy axis (Fig. 10.1) is to align magnetic domains along the easy axis making it a more effective easy axis for which domains are less responsive to the current-induced magnetic field and a higher operating current with higher current-induced magnetic field can be achieved at the expense of a reduction in inductance value as seen in the H-B plot (Fig. 10.1).

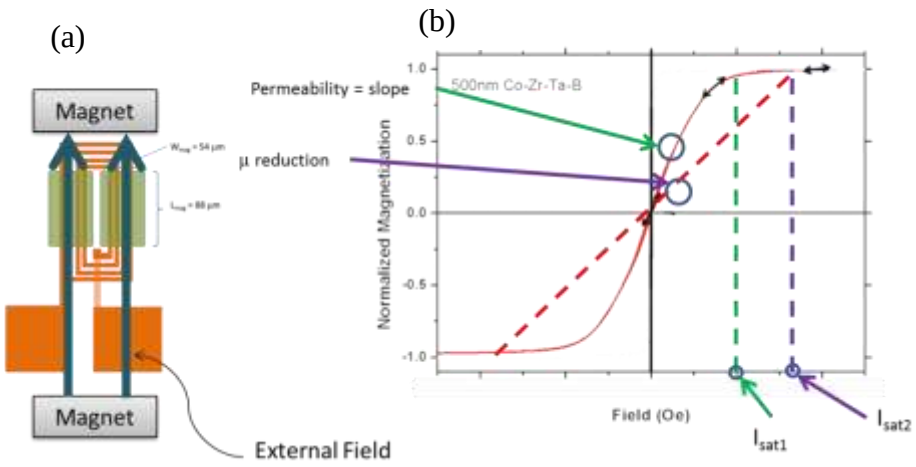

Fig. 10.1: (a) Schematic of Experimental Setup for Investigating the Effect of DC Magnetic Field on Saturation Current (b) Permeability Change and Saturation Current Shift Theorized to Prompt Experimental Effort

10.2 Inductor Characteristics under Simultaneously Applied DC Current and DC Magnetic Field

The DC magnetic field was simultaneously applied with DC currents as it was discussed in the test setup in Chapter 3 and shown in Fig. 4.4. The inductance decreases with the increase in the externally applied DC magnetic field (Fig. 10.2). The physics governing the inductance response is the same physics that is governing the H(Easy) case, discussed in Chapter 5. FMR decreases with large increases in the DC current, as it was discussed in section 9.2 (Fig. 10.1). On the other hand, FMR increases with increases in the DC magnetic field (Fig. 5.5). In the simultaneous case, the decrease in FMR due to the DC current is offset by larger increases in FMR due to the externally applied DC magnetic field (Fig. 10.2).

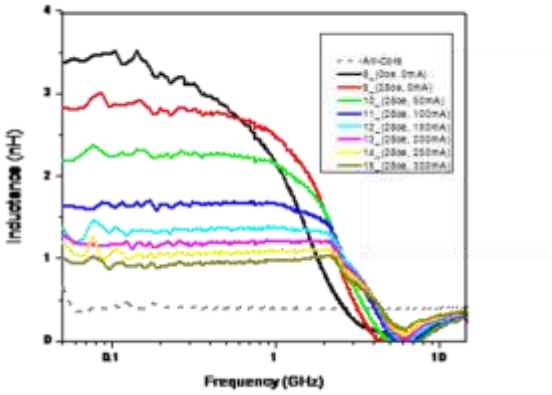

Fig. 10.2: Inductance Response to Simultaneous DC Magnetic Field and DC Current

10.3 Effect of Externally Applied DC Magnetic Field on Current Carrying Capability

The DC magnetic field was simultaneously applied with DC currents as it was discussed in the test setup of Chapter 3 and shown in Fig. 3.5. The quality factor response for the simultaneous condition is reflected in Fig. 10.2. The QF response represented by the red trace in Fig. 10.2 is due to the externally applied magnetic field. The externally applied field increases both PQ and PQF as it was detailed in section 5.1. All other QF responses represent the effect of applying DC magnetic field and DC current simultaneously. The signature of the DC current effect can be seen with an initial increase in PQ followed by a reduction in PQ with increases in currents (Fig. 10.2). Furthermore, PQF increases to maximum values under the simultaneous condition as PQF increases for both; the DC applied field case and the DC current case, independently. Increasing the externally applied magnetic field should increase PQ, PQF and the high-frequency QF response (Fig. 10.3) as discussed in Chapter 6.

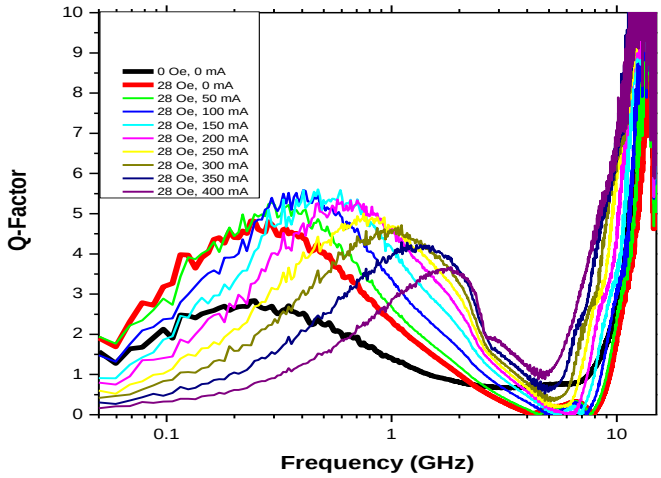

Fig. 10.3: Quality Factor Response to Simultaneous DC Magnetic Field and varying DC Current

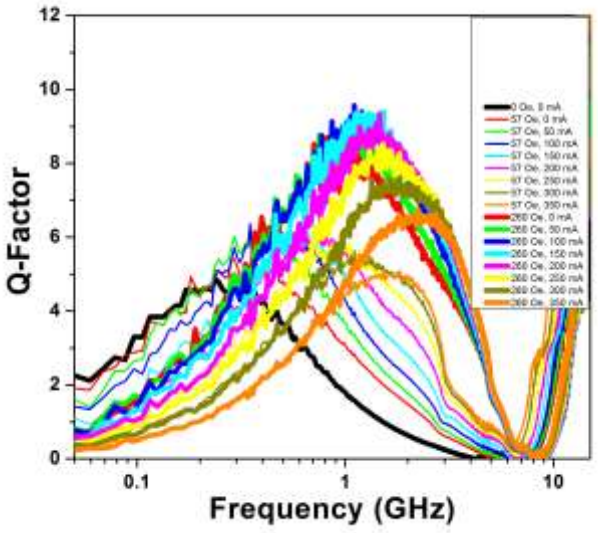

Fig. 10.4 Quality Factor Response to Simultaneous varying DC Magnetic Fields and varying DC Current

To examine the effect of the externally applied DC magnetic field on the current carrying capability experimentally the inductance response of a stripline inductor was examined for simultaneous DC currents and DC magnetic fields (Fig. 10.4) as discussed in the introduction of this chapter. The initial experimental results showed a promising

trend as with an increase in the externally applied DC magnetic field the change in inductance decreased with increases in the operating current on the expense of a reduction in inductance value (i.e. purple trace in Fig. 10.4). To further examine this experimental finding, a new set of simultaneous DC magnetic field with larger DC currents was examined (Fig. 10.5). With larger currents it was expected that the inductance response for the case without the DC field (red trace in Fig. 10.4 and Fig. 10.5) to reach saturation before the simultaneous cases. The experimental results showed that at large operating currents the field independent response (red trace in Fig. 10.5) to converge to the same or larger inductance value of all simultaneous cases.

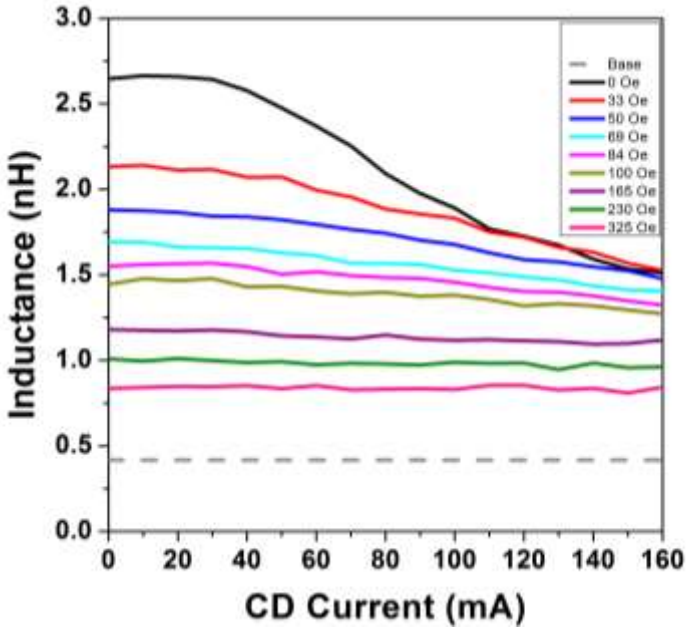

Fig. 10.5: Effect of DC Magnetic Field on Current Carrying Capability and Inductance

10.4 Conclusion

The experimental examination of externally applied DC magnetic field on current carrying capability showed that the rate of decrease in inductance by the current-induced magnetic field reduces with increases in the externally applied magnetic field along the easy axis Fig. 10.6. But at large currents (300 mA), field-independent inductance is equal to that of one with an applied field. At an operating current up to 300 mA, introducing an external DC magnetic field along the easy axis did not provide any benefits in the enhancement of the saturation current. It is suggested to re-conduct the experimental work on power inductors with various magnetic film thicknesses. It is also suggested to re-conduct this experiment at low temperature. At low temperature most carriers freeze out and become less effective. Also lattice vibrations have very minor effects and electron spin dominates with a few dopants. Low temperature experiments should offer more insights on the underlying physics behind the device characteristics. Monte Carlo simulations was used by Diep et. al [43] to produce properties of spin transport in magnetic materials as a function of temperature.

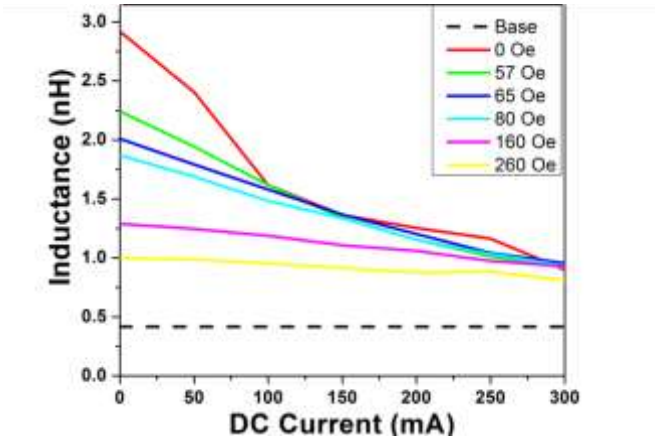

Fig. 10.6: Effect of DC Magnetic Field on Current Carrying Capability (with Larger Currents than previous case)

Chapter 11

CONCLUSIVE REMARKS

11.1 Summary of the Work

This work began by integrating CZTB into on-chip inductor, which resulted in increases in inductance and quality factor. For spiral inductors, there was an increase in PQ from 0.5 to 1.9 (280% increase) and an increase in inductance from 1.9 nH to 7.3 nH. In the stripline inductor case, PQ experienced an increase from 1.8 to 6, which represents an increase of 233. Correspondingly, for stripline inductors, an increase in PQ was experienced from 1.8 to 6. Subsequently, an external DC magnetic field was applied along the easy and hard axes of on-chip inductors to study the effect of spin alignment in the magnetic film on inductor characteristics. The following results are presented relative to a magnetic based inductor without an externally applied field. For spiral inductors, PQ was enhanced from 1.9 to 4.6 (142% increase) and a corresponding increase in PQF from 0.4 GHz to 2.3 GHz. For stripline inductors with a field applied along the easy axis, an increase in PQ from 6 to 12, with a corresponding increase in PQF from 0.3 GHz to 3 GHz was measured. Additionally, along the hard axis, a PQ enhancement was measured from 6 to 10 with an increase in PQF from 0.3 GHz to 2.5 GHz. However, although these enhancements occurred at the expense of inductance, the drops in inductance still resulted in a value that was 50% above the air-core case. Stripline inductors, depending on the selected range of the DC magnetic field (0-650 Oe), PQF increased up to 900% from initial value of 0.5 GHz, and PQ was enhanced up to 118%

above its initial value of 6. But these enhancements came at the expense of inductance reduction.

11.2 Discussion

The results of this study have demonstrated that the integration of a magnetic field on inductors, as well as applying an external field led to significant improvements in a number of inductor characteristics. The role of spin magnetization in magnetic materials is a well understood concept that ultimately leads to the reduction in film resistance. The strength and the orientation of the externally applied field led to these various improvements via series resistance. The figures presented in this work represent a very significant achievement in this field because improvements in quality factor are a highly sought after performance gain. QF is an important metric for highly integrated inductors because it affects phase noise, channel spacing for wireless applications, and frequency planning for other specialty applications. The larger the QF, the less loss is experienced by the electrical system. The increases as determined by this investigation are very large. The significant improvements in PQF enable the capability of operating inductor devices in high-frequency applications. Additionally, magnetic-based inductors tend to degrade in terms of inductance and QF from large DC currents and their corresponding induced fields. It was determined that applying even low DC magnetic fields prevented and reversed degradation effects. It was additionally found that engineering magnetic films so that shape anisotropy overcomes the external magnetic field, resulting in an inductance response that is independent of the applied field.

11.3 Scope of Future Work

Conducting accelerated lifetime (reliability) tests including electrical and thermal stresses with and without the external DC magnetic field, should result in a detailed understanding of the degradation mechanism and the best way to remedy it. Under low temperature conditions, it is suggested that the following is be conducted: first, explore the effect of the external DC magnetic field along the easy and hard axes of on chip inductors, second, examine the influence of the current induced magnetic field on the magnetic film, and third, examine the interaction of externally applied DC magnetic field on current carrying capabilities.

REFERENCES

[1] C. H. Diaz, D. D. Tang, and J. Y. C. Sun, "CMOS technology for MS/RF SoC," *IEEE Transactions on Electron Devices,* vol. 50, pp. 557-566, 2003/03// 2003.

[2] R. Foley, F. Waldron, J. Slowey, A. Alderman, B. Narveson, and S. C. O'Mathuna, "Technology roadmapping for Power Supply in Package (PSiP) and Power Supply on Chip (PwrSoC)," in *2010 Twenty-Fifth Annual IEEE Applied Power Electronics Conference and Exposition (APEC),* 2010, pp. 525-532.

[3] C. P. Yue and S. S. Wong, "On-chip spiral inductors with patterned ground shields for Si-based RF ICs," *IEEE Journal of Solid-State Circuits,* vol. 33, pp. 743-752, 1998/05// 1998.

[4] M. Wens and M. Steyaert, *Design and Implementation of Fully-Integrated Inductive DC-DC Converters in Standard CMOS*, 2011 edition ed. Dordrecht ; New York: Springer, 2011.

[5] J. N. Burghartz and B. Rejaei, "On the design of RF spiral inductors on silicon," *IEEE Transactions on Electron Devices,* vol. 50, pp. 718-729, 2003/03// 2003.

[6] S. A. Chickamenahalli, H. Braunisch, S. Srinivasan, J. He, U. Shrivastava, and B. Sankman, "RF packaging and passives: design, fabrication, measurement, and validation of package embedded inductors," *IEEE Transactions on Advanced Packaging,* vol. 28, pp. 665-673, 2005/11// 2005.

[7] H.-M. Hsu and M.-M. Hsieh, "On-chip inductor above dummy metal patterns," *Solid-State Electronics,* vol. 52, pp. 998-1001, 2008/07// 2008.

[8] C.-C. Tang, C.-H. Wu, and S.-I. Liu, "Miniature 3-D inductors in standard CMOS process," *IEEE Journal of Solid-State Circuits,* vol. 37, pp. 471-480, 2002/04// 2002.

[9] A. L. Adenot, O. Acher, T. Taffary, P. Quéffélec, and G. Tanné, "Tuneable microstrip device controlled by a weak magnetic field using ferromagnetic laminations," *Journal of Applied Physics,* vol. 87, pp. 6914-6916, 2000/05/01/ 2000.

[10] N. Cramer, D. Lucic, R. E. Camley, and Z. Celinski, "High attenuation tunable microwave notch filters utilizing ferromagnetic resonance," *Journal of Applied Physics,* vol. 87, pp. 6911-6913, 2000/05/01/ 2000.

[11] V. Korenivski and R. B. v. Dover, "Magnetic film inductors for radio frequency applications," *Journal of Applied Physics,* vol. 82, pp. 5247-5254, 1997/11/15/ 1997.

[12] J. Mullenix, A. El-Ghazaly, and S. X. Wang, "Integrated Transformers With Sputtered Laminated Magnetic Core," *IEEE Transactions on Magnetics,* vol. 49, pp. 4021-4027, 2013/07// 2013.

[13] J. Qiu, D. V. Harburg, and C. R. Sullivan, "A toroidal power inductor using radial-anisotropy thin-film magnetic material based on a hybrid fabrication process," in *2013 Twenty-Eighth Annual IEEE Applied Power Electronics Conference and Exposition (APEC)*, 2013, pp. 1660-1667.

[14] Z. Ni, J. Zhan, Q. Fang, X. Wang, Z. Shi, Y. Yang, *et al.*, "Design and Analysis of Vertical Nanoparticles-Magnetic-Cored Inductors for RF ICs," *IEEE Transactions on Electron Devices,* vol. 60, pp. 1427-1435, 2013/04// 2013.

[15] X. Yu, M. Kim, F. Herrault, C.-H. Ji, J. Kim, and M. G. Allen, "Silicon-Embedding Approaches to 3-D Toroidal Inductor Fabrication," *Journal of Microelectromechanical Systems,* vol. 22, pp. 580-588, 2013/06// 2013.

[16] A. Zolfaghari, A. Chan, and B. Razavi, "Stacked inductors and transformers in CMOS technology," *IEEE Journal of Solid-State Circuits,* vol. 36, pp. 620-628, 2001/04// 2001.

[17] C. R. Sullivan, "Integrating magnetics for on-chip power: Challenges and opportunities," in *IEEE Custom Integrated Circuits Conference, 2009. CICC '09*, 2009, pp. 291-298.

[18] A. M. Crawford, D. Gardner, and S. X. Wang, "High-frequency microinductors with amorphous magnetic ground planes," *IEEE Transactions on Magnetics,* vol. 38, pp. 3168-3170, 2002/09// 2002.

[19] B. Viala, S. Couderc, A. S. Royet, P. Ancey, and G. Bouche, "Bidirectional ferromagnetic spiral inductors using single deposition," *IEEE Transactions on Magnetics,* vol. 41, pp. 3544-3549, 2005/10// 2005.

[20] B. Viala, A. S. Royet, R. Cuchet, M. Aid, P. Gaud, O. Valls, *et al.*, "RF planar ferromagnetic inductors on silicon," *IEEE Transactions on Magnetics,* vol. 40, pp. 1999-2001, 2004/07// 2004.

[21] K. Kawabe, H. Koyama, and K. Shirae, "Planar inductor," *IEEE Transactions on Magnetics,* vol. 20, pp. 1804-1806, 1984/09// 1984.

[22] M. Yamaguchi, M. Baba, and K. Arai, "Sandwich-type ferromagnetic RF integrated inductor," *IEEE Transactions on Microwave Theory and Techniques,* vol. 49, pp. 2331-2335, 2001/12// 2001.

[23] M. Yamaguchi, S. Arakawa, H. Ohzeki, Y. Hayashi, and K. I. Arai, "Characteristics and analysis of a thin film inductor with closed magnetic circuit structure," *IEEE Transactions on Magnetics,* vol. 28, pp. 3015-3017, 1992/09// 1992.

[24] M. Yamaguchi, K. Suezawa, K. I. Arai, Y. Takahashi, S. Kikuchi, Y. Shimada, *et al.*, "Microfabrication and characteristics of magnetic thin-film inductors in the ultrahigh frequency region," *Journal of Applied Physics,* vol. 85, pp. 7919-7922, 1999/06/01/ 1999.

[25] O. Oshiro, H. Tsujimoto, and K. Shirae, "A Closed-Type Planar Inductor," *IEEE Translation Journal on Magnetics in Japan,* vol. 2, pp. 329-330, 1987/04// 1987.

[26] D. S. Gardner, A. M. Crawford, and S. Wang, "High frequency (GHz) and low resistance integrated inductors using magnetic materials," in *Interconnect Technology Conference, 2001. Proceedings of the IEEE 2001 International*, 2001, pp. 101-103.

[27] H. Wu, D. S. Gardner, W. Xu, and H. Yu, "Integrated RF On-Chip Inductors With Patterned Co-Zr-Ta-B Films," *IEEE Transactions on Magnetics,* vol. 48, pp. 4123-4126, 2012/11// 2012.

[28] H. Wu, S. Zhao, D. S. Gardner, and H. Yu, "Improved High Frequency Response and Quality Factor of On-Chip Ferromagnetic Thin Film Inductors by Laminating and Patterning Co-Zr-Ta-B Films," *IEEE Transactions on Magnetics,* vol. 49, pp. 4176-4179, 2013/07// 2013.

[29] H. Wu, S. Zhao, D. S. Gardner, and H. Yu, "Aspect ratio dependent saturation field in patterned amorphous Co-Zr-Ta-B thin films with uniaxial anisotropy," *Journal of Applied Physics,* vol. 115, 2014/05/07/ 2014.

[30] H. Wu, D. S. Gardner, S. Zhao, H. Huang, and H. Yu, "Control of magnetic flux and eddy currents in magnetic films for on-chip radio frequency inductors: Role of the magnetic vias," *Journal of Applied Physics,* vol. 115, 2014/05/07/ 2014.

[31] S. Azeemuddin, A. Hoffmann, R. Divan, M. J. Donahue, S. H. Chung, and P. Wang, "High-Frequency Domain-Wall Motion and Magnetization Rotation of Patterned Permalloy Films under External Magnetic Field Excitation," in *Sixth IEEE Conference on Nanotechnology, 2006. IEEE-NANO 2006*, 2006, pp. 853-856.

[32] J. Kim, W. Ni, C. Lee, E. C. Kan, I. D. Hosein, Y. Song, *et al.*, "Magnetic property characterization of magnetite (Fe3O4) nanorod cores for integrated solenoid rf inductors," *Journal of Applied Physics,* vol. 99, 2006/04/15/ 2006.

[33] Y. Zhuang, M. Vroubel, B. Rejaei, and J. N. Burghartz, "Integrated RF inductors with micro-patterned NiFe core," *Solid-State Electronics,* vol. 51, pp. 405-413, 2007/03// 2007.

[34] I. Žutić, J. Fabian, and S. Das Sarma, "Spintronics: Fundamentals and applications," *Reviews of Modern Physics,* vol. 76, pp. 323-410, 2004/04/23/ 2004.

[35] C. Kittel, "On the Theory of Ferromagnetic Resonance Absorption," *Physical Review,* vol. 73, pp. 155-161, 1948/01/15/ 1948.

[36] H. Wu, H. Yu, B. Bakkaloglu, Y. Cao, S. Chickamenahalli, and U. Arizona State, "Integrated Inductors with Micro-Patterned Magnetic Thin Films for RF and Power Applications," in *ASU Electronic Dissertations and Theses*, ed: Arizona State University, 2013.

[37] T. Dastagir, W. Xu, S. Sinha, H. Wu, Y. Cao, and H. Yu, "Tuning the permeability of permalloy films for on-chip inductor applications," *Applied Physics Letters,* vol. 97, 2010/10/18/ 2010.

[38] D. S. Gardner, G. Schrom, P. Hazucha, F. Paillet, T. Karnik, S. Borkar, *et al.*, "Integrated On-Chip Inductors with Magnetic Films," in *Electron Devices Meeting, 2006. IEDM '06. International*, 2006, pp. 1-4.

[39] P. R. Morrow, C.-M. Park, H. W. Koertzen, and J. Dibene, "Design and Fabrication of On-Chip Coupled Inductors Integrated With Magnetic Material for Voltage Regulators," *IEEE Transactions on Magnetics,* vol. 47, pp. 1678-1686, 2011/06// 2011.

[40] P. Herget, N. Wang, E. J. O'Sullivan, B. C. Webb, L. T. Romankiw, R. Fontana, *et al.*, "A Study of Current Density Limits Due to Saturation in Thin Film Magnetic Inductors for On-Chip Power Conversion," *IEEE Transactions on Magnetics*, vol. 48, pp. 4119-4122, 2012/11// 2012.

[41] W. Xu, H. Wu, D. S. Gardner, S. Sinha, T. Dastagir, B. Bakkaloglu, *et al.*, "Sub-100 μm scale on-chip inductors with CoZrTa for GHz applications," *Journal of Applied Physics*, vol. 109, 2011/04/01/ 2011.

[42] M. Julliere, "Tunneling between ferromagnetic films," *Physics Letters A*, vol. 54, pp. 225-226, 1975/09/08/ 1975.

[43] H. T. Diep, Y. Magnin, and D.-T. Hoang, "Spin Resistivity in Magnetic Materials," *Acta Physica Polonica A,* vol. 121, pp. 985-991, 2012/06//MAY 2012.